Techno-Economic and Sustainability Assessment of a Circular Two-Stage Olive Mill Wastewater Treatment System Using Olive Pomace-Derived Activated Carbon

Raid Alrowais [a,*] Mahmoud M. Abdel daiem [b,*] Rania Saber Yousef,[c] Osama konsowa Ahmed,[c] Amany A. Metwally [d] and Noha Said [b]

This study presents a sustainable and cost-effective approach for treating olive mill wastewater (OMWW) using activated carbon derived from olive pomace, a major by-product of olive oil production. The proposed system integrates the production of this adsorbent with wastewater treatment in a two-stage, circular process that combines acid precipitation and adsorption. The prepared activated carbon exhibited a well-developed porous structure and high iodine value (948 mg/g), enabling efficient removal of phenolic compounds from OMWW. The results showed removal efficiencies exceeding 99% for phenolic compounds, along with significant reductions in key pollutants, including chemical oxygen demand and total organic carbon. It was hypothesized that integrating waste valorization with wastewater treatment can enhance both environmental and economic performance. The findings confirmed this hypothesis, demonstrating high treatment efficiency and substantial cost reduction through process optimization, including reduced adsorbent dosage and reuse. Process optimization, including reduced adsorbent dosage and reuse, led to a substantial decrease in treatment costs. Overall, this study demonstrated that integrating waste valorization with wastewater treatment offers an effective and practical solution for environmental management. The findings highlight the potential of olive pomace-derived activated carbon as a low-cost and sustainable adsorbent for large-scale applications.

DOI: 10.15376/biores.21.2.4977-5009

Keywords: Waste valorization; Adsorption; Phenolic removal; Sustainable treatment; SDG 6: Clean water and sanitation; SDG 9: Industry; Innovation and infrastructure

*Contact information: a: Department of Civil Engineering, College of Engineering, Jouf University, Sakakah 72388, Saudi Arabia; b: Environmental Engineering Department, Faculty of Engineering, Zagazig University, Zagazig, 44519, Egypt; c: Biochemistry Department, Faculty of Agriculture, Cairo University, Giza, 12613, Egypt; d: Agricultural Engineering Department, Faculty of Agriculture, Zagazig University, Zagazig, 44511, Egypt; * Corresponding authors: rnalrowais@ju.edu.sa; mmabdeldaiem@eng.zu.edu.eg*

INTRODUCTION

Olive cultivation is a significant global agricultural activity, covering nearly ten million hectares and yielding more than 3.30 million tons per year of olive oil, with Mediterranean countries producing around 95% of the world's supply (Foti *et al*. 2021; IOC 2024). This sector plays a vital socio-economic role in many rural economies, supporting millions of livelihoods and driving regional agro-industrial development (Kurtoğlu *et al*. 2024). In recent years, olive production has also expanded in regions such

as Saudi Arabia, contributing to increased production capacity and economic value (IMARC 2024).

Despite its economic importance, the olive oil extraction process produces substantial quantity of liquid and solid waste, with olive mill wastewater (OMWW) being the most problematic by-product (Roque *et al*. 2025). OMWW is a dark, malodorous effluent with an extremely high load of organics, elevated salinity, and a wide array of phenolic compounds that exhibit strong antimicrobial, phytotoxic, and antioxidant properties (Dahdouh *et al*. 2023; Roque *et al*. 2025). Global OMWW generation is estimated at 10 to 30 million cubic meters annually, posing serious environmental risks when discharged untreated (Annab *et al*. 2019; Di Giacomo and Romano 2022). Its complex composition and seasonal generation further complicate treatment and disposal (Alrowais *et al*. 2023a; Dali *et al*. 2023; Dich *et al*. 2025).

The environmental impact of OMWW is mainly associated with its high concentration of recalcitrant phenolic compounds, which inhibit biological treatment processes (Ayadi *et al*. 2022; Alrowais *et al*. 2023c). Conventional treatment methods, including physical, chemical, and biological processes, have been widely investigated (Bottino *et al*. 2020; Posadino *et al*. 2021; Awadallah *et al.* 2023; Benaddi *et al*. 2023; Abu-Dalo *et al*. 2024; Jamrah *et al*. 2024). However, these approaches are often limited by high costs, energy requirements, inconsistent efficiency, and the generation of secondary waste (El Shahawy *et al*. 2021).

The motivation for this study is to develop an integrated, low-cost, and sustainable solution that aligns with circular-economy principles while addressing the environmental challenges associated with OMWW. Adsorption has emerged as an effective method for removing phenolic compounds, particularly using activated carbon (AC) (Abu-Dalo *et al*. 2024). However, commercial AC is expensive and energy-intensive, limiting its large-scale application (Okpara *et al*. 2023; Abd El-wahaab *et al*. 2025). Therefore, there is growing interest in developing low-cost adsorbents from agricultural residues. Olive pomace (OP), a major by-product of olive oil production, is an abundant and carbon-rich material suitable for AC production, offering a promising pathway for waste valorization (Alrowais *et al*. 2023b, 2024; Abd El-wahaab *et al*. 2025).

Previous studies have demonstrated the effectiveness of olive-residue-derived AC for phenolic removal, often achieving efficiencies exceeding 80% and favorable adsorption behavior (Raupp *et al*. 2021; Bougheriou and Ghoualem 2023; Djeziri *et al*. 2023). However, most studies focus either on adsorbent preparation or wastewater treatment separately. In addition, acid precipitation has been shown to partially remove phenolic compounds but requires further treatment to achieve complete detoxification (Alrowais *et al*. 2023c).

Despite these advances, a clear research gap remains in integrating waste valorization with OMWW treatment within a unified circular framework. Existing studies typically focus either on producing AC without direct application to OMWW (Raupp *et al*. *2021*; Bougheriou and Ghoualem 2023; Djeziri *et al.* 2023) or on using non-integrated treatment systems (Bottino *et al.* 2020; Benaddi *et al.* 2023; Abu-Dalo *et al.* 2024; Jamrah *et al.* 2024). To address this gap, this study proposes a novel two-stage treatment system combining acid precipitation and adsorption using activated carbon derived from olive pomace (OP-AC). The main objective was to develop a sustainable and economically viable solution that simultaneously manages solid and liquid waste streams. In addition, this work included a comprehensive techno-economic and sustainability assessment to evaluate its practical applicability.

Importantly, this study was the first to integrate a comprehensive techno-economic evaluation with OP-AC based OMWW treatment, demonstrating the conversion of an environmental liability into a profitable circular process. The main contributions of this work can be summarized as follows:

(i) valorization of olive pomace into a low-cost, high-performance AC,
(ii) development of a circular two-stage treatment system for efficient OMWW detoxification, and
(iii) evaluation of techno-economic feasibility and sustainability for practical implementation.

EXPERIMENTAL

The methodology of this study integrated the valorization of OP with the treatment of OMWW within a circular, zero-waste framework. First, raw OMWW collected from olive processing units was characterized for key physicochemical and inorganic parameters, including total solids (TS), electric conductivity (EC), total organic carbon (TOC), chemical oxygen demand (COD), biological oxygen demand (BOD), total phenolic compounds (TPh), and major cations (K^+, Na^+, Fe^{3+}, Cu^{2+}, Mn^{2+}, Zn^{2+}). OP, generated as the main solid residue of the olive oil production process, was utilized as the precursor for OP-AC production. The fabrication involved drying the pomace, chemical impregnation using H_3PO_4, pyrolysis at 450 °C under nitrogen flow, followed by washing and final drying. The OP-AC was comprehensively characterized using multiple analytical techniques, including surface area and pore structure analysis, TGA/DTG thermal stability assessment, FTIR functional group identification, SEM morphological imaging, proximate/ultimate analysis, and elemental composition (Energy-Dispersive X-ray Spectroscopy (EDX)/XRF). Adsorption experiments were then performed to evaluate kinetics, isotherms, and the effect of pH and temperature on phenolic compounds removal from OMWW. Finally, an integrated treatment approach was applied, consisting of acid precipitation (T1) at pH 2.6 to induce coagulation–sedimentation, followed by OP-AC adsorption (T2) to remove dissolved organics, phenolic compounds, and metals. The combined system was evaluated for treatment efficiency across all parameters, demonstrating the synergistic performance of precipitation and adsorption in OMWW purification. Figure 1 indicates the flow chart of the methodology used in the current work.

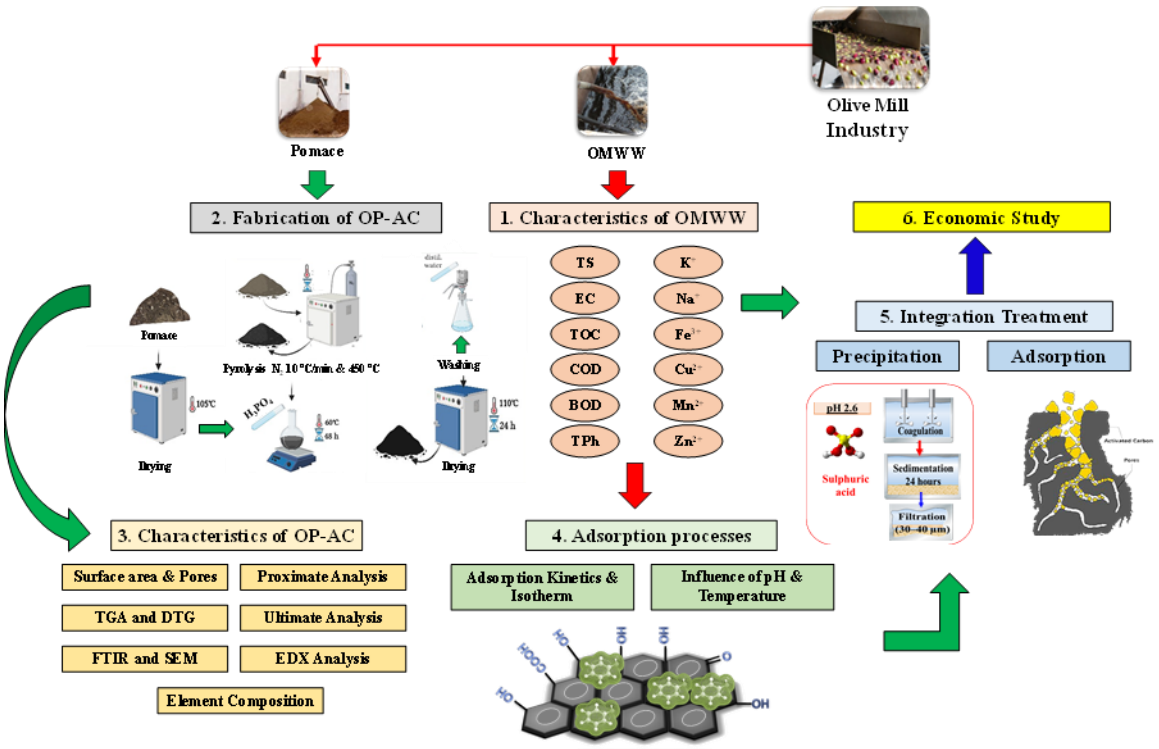

Fig. 1. Methodology flowchart of the current study

Raw Materials and Chemicals

The OP was collected from a local olive-processing facility in the Al-Jouf region, Saudi Arabia. The material was transported in sealed containers and stored at room temperature before processing. OMWW samples were obtained from the same facility during peak production season. All chemicals used in the study, including phosphoric acid (H_3PO_4, 85%), sodium hydroxide (NaOH), and Folin–Ciocalteu reagent, were of analytical purity and supplied by Sigma-Aldrich.

Preparation of OP-AC

The collected OP was initially dried at 105 °C for 24 h to eliminate residual moisture. The dried material was then ground using a laboratory mill and then sieved to retain particles with a size below 1 mm. The resulting powder was washed with distilled water several times to remove soluble impurities, and then it was dried again before activation. Chemical activation was performed by impregnating approximately 100 g of the pre-treated pomace with phosphoric acid (H_3PO_4) at a weight ratio of 1:3 (pomace: H_3PO_4), ensuring thorough mixing for uniform penetration of the activating agent (Abdel daiem *et al*. 2019; Mohammad *et al*. 2022). The impregnated samples were subsequently carbonized at 450 °C for 30 min and washed repeatedly with distilled water to achieve a filtrate pH of around 6. Finally, the AC was dried at 105 °C for 24 h and preserved in airtight containers for subsequent use.

Characterization of OP-AC

Surface functional groups were identified through Fourier Transform Infrared (FTIR) spectroscopy using a PerkinElmer Spectrum (PerkinElmer Inc., Waltham, MA, USA) operating across a wavenumber range of 4000 to 550 cm^{-1}. Surface morphology and

pore structure were examined *via* Scanning Electron Microscopy (SEM) using a JEOL JSM-6510LV scanning electron microscope (JEOL Ltd., Tokyo, Japan). In contrast, textural properties, including specific surface area, pore diameter, and pore volume, were quantified using Brunauer–Emmett–Teller (BET) adsorption analysis performed on a Micromeritics ASAP 2020 surface area and porosity analyzer (Micromeritics Instrument Corp., Norcross, GA, USA). The crystallographic structure of the OP-AC was determined by X-ray diffraction (XRD) using a Shimadzu XRD-6000 diffractometer (Shimadzu Corporation, Kyoto, Japan), equipped with an X-ray generator operated at 40 kV and 25 mA, employing monochromatic Cu $K\alpha_1$ radiation (λ = 1.54178 Å). Diffraction patterns were recorded over a 2θ range of 2°–70°.

Thermogravimetric analysis (TGA) and derivative thermogravimetric (DTG) measurements were performed using a Shimadzu TGA-50H thermal analyzer (Shimadzu Corporation, Kyoto, Japan) over a temperature range of (30 to 600 °C) at a heating rate of 10 °C/min and a nitrogen flow of 30 mL/min. The ash content, defined as the non-combustible inorganic residue, was determined by subjecting approximately 1.0 g of the adsorbent in a Nabertherm L 9/11 muffle furnace (Nabertherm GmbH, Lilienthal, Germany) at 1000 °C for one hour. The mass of the residue was measured after the crucible had cooled down.

The iodine value serves as an essential indicator of an adsorbent's microporosity and overall pore characteristics and is widely used to assess the quality of AC (Djeziri *et al*. 2023). To determine the iodine adsorption capacity, 10 mL of 0.01 N iodine solution was first titrated with 0.1 N sodium thiosulfate using starch as an indicator until the endpoint was reached. After filtration, 0.05 g of the AC was added to 15 mL of 0.1 N iodine solution and stirred for 5 minutes. The mixture was filtered, and the remaining iodine in the filtrate was titrated with 0.1 N sodium thiosulfate in the presence of a starch indicator until decolorization occurred, allowing calculation of the iodine adsorption capacity. The yield of AC, which reflects the efficiency of the conversion process from raw biomass, is highly dependent on factors including the precursor material and activation parameters (Bougheriou and Ghoualem 2023). The yield was determined according to Eq. 1:

$$Y(\%) = \frac{\text{Mass of AC obtained}}{\text{Mass of raw material used}} \times 100 \quad (1)$$

Characterization of OMWW

A comprehensive physicochemical characterization of the OMWW samples was conducted. Parameters including TS, COD, BOD, and TOC were measured following standard methods (APHA, 2005). The solution pH and electrical conductivity (EC) were determined using a portable meter (HI 98107). Furthermore, the concentrations of specific elements (Na^+, K^+, Fe^{3+}, Cu^{2+}, Mn^{2+}, Zn^{2+}) were analyzed by atomic absorption spectrometry (Fisher Scientific ICE 3000). Phenolic compounds were quantified using the Folin–Ciocalteu method, with gallic acid employed as an external calibration standard (Medina 2011). Following the designated contact period, the mixtures were filtered, and the remaining phenolic compound concentration in the filtrate was determined using a UV–Vis spectrophotometer at absorbance wavelength (λ_{max} = 760 nm).

Adsorption Experiments

Adsorption experiments were conducted to evaluate the influence of pH, adsorbent dosage, contact time, and temperature on the removal efficiency of phenolic compounds

under continuous magnetic stirring. In each experimental run, 100 mL of phenolic solution with an initial concentration of 500 mg/L was used. The raw OMWW contained approximately 5000 mg/L of phenolic compounds, and the working solution (500 mg/L) was obtained by dilution (1:10). All optimization experiments were conducted using diluted real OMWW, not synthetic solutions. The mixture was then introduced to OP-AC and subjected to controlled agitation to ensure effective contact between the adsorbent and solute.

Adsorption Kinetics

The kinetic study was carried out to evaluate the adsorption equilibrium time. A carbon mass of 1.0 g was introduced into 100 mL Erlenmeyer flasks containing diluted OMWW (1:10), yielding an initial concentration (500 mg/L) of total phenolic compounds (TPh). The solution pH was kept at its natural level without adjustment. The adsorption kinetics were analyzed using established models (Eqs. 2 and 3), and the intraparticle diffusion approach (Eq. 4) was adopted to assess if pore diffusion was the rate-limiting step, as described in previous research by Aljubiri *et al*. (2024a,b).

$$q = q_{\text{pred},1}\left(1 - e^{-k_1 t}\right) \tag{2}$$

$$q = \frac{q_{\text{pred},2}^2 \mathrm{k}_2 \mathrm{t}}{1 + q_{\text{pred},2} \mathrm{k}_2 \mathrm{t}} \tag{3}$$

$$q = \mathrm{k}_{\text{id}}\, \mathrm{t}^{1/2} + \mathrm{C} \tag{4}$$

where q is adsorption yield (mg/g); $q_{\text{pred},1}$ is the predicted adsorption yield in the first-order kinetic model (mg/g); $q_{\text{pred},2}$ is the predicted adsorption yield in the second-order kinetic model (mg/g); k_1 is the rate of adsorption for the first-order (L/min); k_2 is the second-order constant (g/mg/min); and t is the time in h. k_{id} is intraparticle diffusion rate constant (mg/g/min), and C is boundary layer thickness constant.

To assess the kinetic models, the average absolute percentage deviation (%D) was calculated according to Eq. 5,

$$\%D = \frac{1}{N}\sum_{\mathrm{i}=1}^{N}\left|\frac{q_{\text{exp}} - q_{\text{pred}}}{q_{\text{exp}}}\right| \times 100\% \tag{5}$$

where N is the number of experiments; and q_{exp} and q_{Pred} denote the experimental and predicted adsorption yields (mg/g).

Adsorption Isotherm

Adsorption isotherms were determined using varying carbon masses (100 to 2000 mg) with an OMWW solution that had an initial phenolic compound concentration of 500 mg/L following a 1:10 dilution. The adsorption behavior was interpreted by fitting the experimental data to the Langmuir, Freundlich, and Prausnitz-Radke isotherm models (Eqs. 6 to 8) to elucidate the adsorption mechanism and type.

$$X_{\text{eq}} = \frac{BX_{\text{m}}C_{\text{e}}}{1 + BC_{\text{e}}} \tag{6}$$

$$X_{\text{eq}} = K_{\text{F}} C_{\text{e}}^{1/nF} \tag{7}$$

$$q = \frac{aC_A}{1+bC_A{}^{\beta}} \quad (8)$$

where X_{eq} represents adsorption yield (mg/g); X_m is adsorption capacity (mg/g); B is a constant of Langmuir yield (L/mg); C_e is the pollutant equilibrium concentration (mg/L); $1/n_F$ is the AC surface heterogeneity; K_F is the relative adsorption capacity; and a (L/g), b (L^{β}/mg^{β}), and β are constants.

Integrated Detoxification System

The integrated detoxification system was designed to reduce the phytotoxicity associated with the high phenolic content of OMWW. The treatment (T) process was implemented in two sequential stages: (A) T1: acid precipitation of OMWW, followed by (B) T2: adsorption using OP-AC, a major solid residue of olive oil production. This dual-stage approach intends to either recover or eliminate phenolic compounds, which, despite their strong antioxidant and bioactive properties, exhibit significant toxicity to plants and microbial communities. Effective phenolic compounds removal can be enhanced by integrating complementary physicochemical processes, with physical methods playing an important role in maximizing extraction and detoxification efficiency (Tundis *et al*. 2021).

Acid precipitation (T1) was performed by lowering the pH of raw OMWW from approximately 4.5 to 2.6 using concentrated sulfuric acid (95% to 98%), thereby promoting coagulation and sedimentation of suspended solids in accordance with Stokes' law (Bazzarelli *et al*. 2015). This physicochemical treatment destabilizes colloidal particles, facilitating their agglomeration into filterable flocs. The presence of inorganic metal ions such as Fe^{2+}, Fe^{3+}, Cu^{2+}, and Zn^{2+} further enhances the formation of coagulant–metal complexes, which precipitate as insoluble aggregates. Phenolic compounds, comprising aromatic rings with hydroxyl functional groups, also participate in this process; under strongly acidic conditions, they undergo charge neutralization, which reduces their solubility and promotes their removal (Hecini and Achour 2014; Grioui *et al*. 2023). Polyfunctional tannins containing multiple dihydroxyphenyl groups additionally act as natural chelating agents, facilitating the precipitation of metal–phenolic complexes. After overnight settling, the OMWW was subjected to sequential filtration through a nylon filter followed by a wire mesh filter of pore size (30 to 40 μm). The system operated at ambient pressure and at a controlled temperature of 25 ± 1 °C, with continuous acid dosing throughout the process to maintain the target pH.

Economic Study Methodology

The economic study was conducted to evaluate the financial feasibility of the proposed two-stage OMWW treatment system based on T1 followed by T2 using OP-AC. The analysis was performed at a representative pilot-to-industrial scale, assuming an olive mill treating 1000 m^3 of OMWW per year and generating approximately 10 tons of dry OP annually (Roig *et al*. 2006).

Cost Estimation Framework

A bottom-up cost estimation approach was applied, in which all relevant operating costs were identified and quantified. These included:

(i) OP-AC production costs (drying, chemical activation, pyrolysis energy, washing, labor, and maintenance) (Wright *et al*. 2010; Manyà 2012), and

(ii) OMWW treatment costs associated with acid precipitation (chemical consumption and handling) and adsorption (OP-AC consumption, energy, and filtration) (Qasim 2017).

Capital investment costs were excluded, as the focus of the study was on operational feasibility and comparative economic performance. All costs were calculated and reported exclusively in Saudi Riyal (SAR) based on prevailing local prices and typical industrial operating conditions (Ouda 2013; MARAFIQ 2025; SERA 2025).

Treatment Cost Calculation

The treatment cost per cubic meter of OMWW was calculated using Eq. 9:

$$C_t = C_{T1} + C_{T2} \quad (9)$$

where C_t is the total treatment cost (SAR/m³), C_{T1} represents the cost of acid precipitation, and C_{T2} represents the cost of OP-AC adsorption.

Two operational scenarios were evaluated: (i) an unoptimized scenario, assuming a conservative OP-AC dosage (Foo and Hameed 2010), and (ii) an optimized scenario, incorporating reduced adsorbent dosage and multiple regeneration–reuse cycles based on experimental adsorption performance (Ahmed and Hameed 2020).

Economic Benefits and Avoided Costs

Economic benefits were quantified by identifying avoided or offset costs resulting from the implementation of the treatment system. These included avoided OMWW disposal expenses, avoided regulatory penalties associated with environmental non-compliance, and the economic value of treated water reused for irrigation. Additional value was attributed to the circular valorization of OP through its conversion into OP-AC. The total annual economic benefit was calculated as the sum of these avoided and generated values and compared against total yearly operating costs (Niaounakis and Halvadakis 2006; Jarboui *et al*. 2008; Qadir *et al*. 2020).

Economic Performance Indicators

Overall economic performance was assessed using annual net balance and net profit indicators, calculated as the difference between total annual benefits and total annual costs. Sensitivity to process optimization was evaluated by comparing unoptimized and optimized scenarios to identify the dominant cost drivers and the conditions under which the treatment system becomes economically viable.

RESULTS AND DISCUSSION

Characteristics of OP-AC

Table 1 provides an in-depth characterization of OP-AC. The OP-AC sample showed BET surface area (24.2 m²/g) and total pore volume (0.08 cm³/g), indicating a predominantly mesoporous structure with a mean pore diameter of 13.9 nm. These textural properties suggest that the material favors adsorption of larger molecules rather than micropore-driven uptake. The strongly negative zeta potential (–28.1 mV) reflected good colloidal stability and a negatively charged surface, which enhances adsorption of positively charged species in aqueous systems (Aljubiri *et al*. 2024a,b). The proximate analysis showed an exceptionally low moisture content (0.03%). A similar value was

reported by Djeziri *et al*. (2023). The ash content of 9.1% was within the expected range for lignocellulosic precursors and consistent with the ash content of ACs that has been reported by Bougheriou and Ghoualem (2023) and Alcazar-Ruiz *et al*. (2024). This ash fraction corresponds to the presence of inherent minerals, which may influence adsorption behavior, particularly for ionic or polar organic compounds.

The carbon content of 60.6% indicates effective thermal activation, aligning with the results obtained by Grioui *et al*. (2023) and Chafi *et al*. (2025), while the measured hydrogen (4.83%) and nitrogen (2.60%) levels imply the retention of surface functional groups capable of engaging in hydrogen bonding and electrostatic interactions with phenolic compounds (Raupp *et al*. 2021; Alouiz *et al*. 2024; Ramos *et al.* 2025). A particularly noteworthy feature of the synthesized AC is its high iodine value (948 mg/g), which reflects a well-developed microporous structure, consistent with the high adsorption capacities reported by Bougheriou and Ghoualem (2023), Djeziri *et al*. (2023), and Alouiz *et al*. (2024). The activation yield of 61% is also consistent with chemically activated biomass (50% to 65%) and demonstrated the economic viability of H_3PO_4 activation (Raupp *et al*. 2021; Bougheriou and Ghoualem 2023; Alouiz *et al*. 2025b). Elemental composition analysis revealed a mineral matrix dominated by silicon (25.0%), aluminum (5.6%), calcium (5.1%), chlorine (7.1%), and iron (4.1%). The presence of phosphorus (4.72%) and sulfur (2.09%) reflects both inherent biomass composition and residues from phosphoric-acid activation (Alouiz *et al*. 2025b). Trace metals such as Zn, Mo, Ti, Sr, and Zr appeared in low concentrations, consistent with reported olive-pomace ash profiles. Their presence does not negatively affect adsorption and, in some cases, can enhance catalytic or surface redox properties (Alcazar-Ruiz *et al*. 2024; Alouiz *et al*. 2024).

The oxide composition further validates the mineralogical structure of AC. Silica (SiO_2) dominated at 53.6%, consistent with previously reported by Grioui *et al*. (2023). Al_2O_3 (10.5%) and P_2O_5 (10.8%) fell within the ranges associated with biomass activated with phosphoric acid, supporting the presence of acidic functional sites that contribute to enhanced phenolic compounds adsorption (Alouiz *et al*. 2024). The measured levels of iron oxide (FeO) and sulfur trioxide (SO_3), each present at roughly 5%, were consistent with concentrations previously documented in similar AC materials by Grioui *et al*. (2023). The presence of CaO, K_2O, and ZnO complements the surface reactivity profile and aligns with findings from comparable olive-waste adsorbents (Alouiz *et al*. 2025b).

Overall, the physicochemical and mineralogical characteristics of the synthesized OP-AC compared favorably with, and in several aspects exceed, those reported in the literature for olive-pomace-based and other biomass-derived ACs. The combination of high microporosity, substantial carbon content, favorable functional groups, and diverse metal oxide composition demonstrates that the OP-AC is a high-performance, low-cost, and ecofriendly adsorbent suitable for the effective reduction of phenolic compounds from OMWW. These results support the broader application of OP valorization within circular-economy frameworks targeting waste minimization and environmental protection in olive-oil-growing area.

Table 1. Characteristics of OP-AC

Textural Properties and Surface Charge Characteristics													
Surface Area (m^2/g)		Total Pore Volume (cm^3/g)		Mean Pore Diameter (nm)		Zeta Potential (mV)		Iodine Value (mg/g)					
24.21		0.08		13.87		-28.12		948.00					
Proximate and Ultimate Analyses													
MC (%)		Ash (%)		C (%)		H (%)		N (%)					
0.03		9.10		60.59		4.83		2.60					
Elemental Composition (EDX Analysis) (%)													
Al	Ca	Cl	Fe	K	Mo	Nb	P	S	Si	Sr	Ti	Zn	Zr
5.55	5.10	7.06	4.05	1.74	0.19	0.18	4.72	2.09	25.05	0.05	0.52	0.39	0.08
Oxide Composition (%)													
Al_2O_3	CaO	Cl	FeO	K_2O	MoO_3	Nb_2O_5	P_2O_5	SO_3	SiO_2	SrO	TiO_2	ZnO	ZrO_2
10.49	7.14	7.06	5.21	2.10	0.29	0.26	10.82	5.22	53.59	0.06	0.87	0.49	0.11

FTIR Analysis of OP-AC

The FTIR spectrum of the synthesized OP-AC (Fig. 2) reveals several characteristic absorbance bands, confirming the presence of oxygenated surface functional groups typically associated with chemically activated lignocellulosic carbons (Chafi *et al*. 2025). The broad band appearing near 3420 cm^{-1} corresponds to O–H stretching vibrations, which are generally assigned to hydroxyl groups in alcohols, phenolic compounds, residual lignocellulosic structures, or physically adsorbed water (Kiełbasa *et al*. 2022). The persistence of this band after carbonization suggests incomplete dehydration and the retention of hydrophilic functionalities known to enhance adsorption through hydrogen bonding (Metyouy *et al*. 2024).

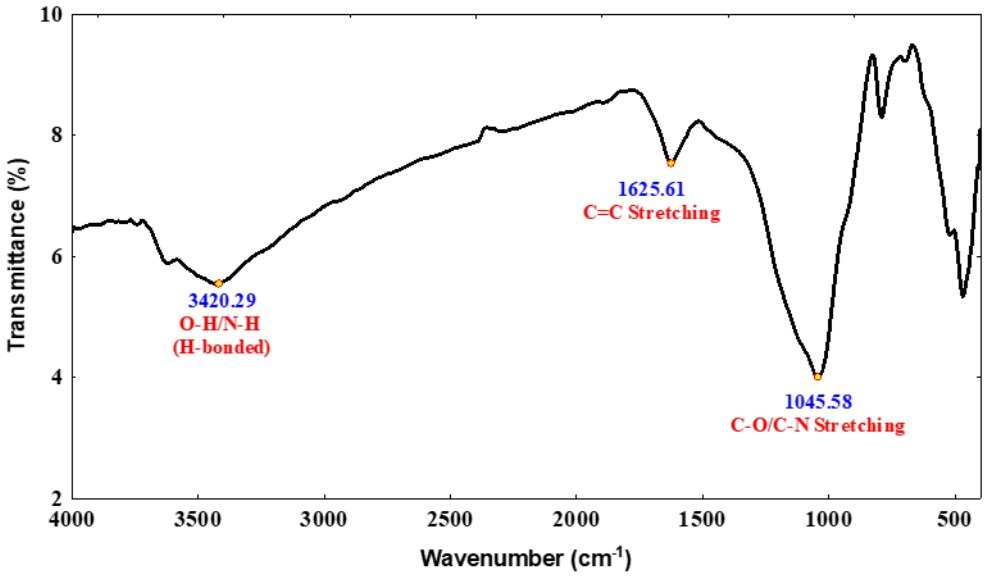

Fig. 2. FTIR profile of OP-AC

A pronounced absorbance band around 1625.6 cm^{-1} is attributed to C=C stretching vibrations of aromatic structures, combined with possible O–H bending modes of bound water (Ramos *et al*. 2025). This band reflects the development of aromaticity during carbonization, confirming the formation of a stabilized carbon matrix while still maintaining oxygenated functionalities that are crucial for phenolic compound interactions in OMWW. The band observed near 1045.6 cm^{-1} corresponds to C–O stretching vibrations, which are typically associated with alcohols, carboxylic acids, esters, or residual polysaccharide structures (Alouiz *et al*. 2025b). This region is characteristic of thermochemically ACs where phosphoric acid promotes cross-linking and stabilizes oxygenated structures. Finally, the peaks appearing around 780 to 890 cm^{-1} are indicative of aromatic C–H out-of-plane bending, confirming the presence of substituted aromatic rings within the carbon framework (Grioui *et al*. 2023). These bands collectively suggest that aromaticity is well-developed, yet the carbon retains numerous polar functional groups, consistent with the behavior of H_3PO_4-activated biomass (Bougheriou and Ghoualem 2023).

Overall, the FTIR profile demonstrates that the AC surface was enriched with O–H, C=O, C–O, and aromatic C=C functionalities, all of which enhanced its polarity and adsorption potential. These groups promote strong interactions with phenolic compounds through mechanisms such as hydrogen bonding and electrostatic attraction, and key

processes governing OMWW detoxification. Similar spectral characteristics have been reported for phosphoric-acid-activated olive residues and other agricultural biomasses (Raupp *et al*. 2021; Metyouy *et al*. 2024; Alouiz *et al*. 2025b), confirming the effective activation and the suitability of this material for phenolic adsorption applications.

Thermogravimetric Analysis of OP-AC

The TGA and DTG curves of the OP-AC provide valuable insight into the material's thermal behavior, as shown in Fig. 3. In the low-temperature region below approximately 150 °C, the TGA profile shows a minor weight loss related to the evaporation of physically adsorbed water and the release of light volatile compounds (Abu-Dalo *et al*. 2023). This initial mass reduction is supported by a small DTG peak and is characteristic of OP-AC that retains a limited quantity of moisture due to the presence of hydroxyl and other oxygenated surface groups (Alcazar-Ruiz et al. 2024; Ramos *et al*. 2025). The relatively low mass loss in this stage reflects the adequate pre-drying and effective carbonization of the raw olive pomace during chemical activation.

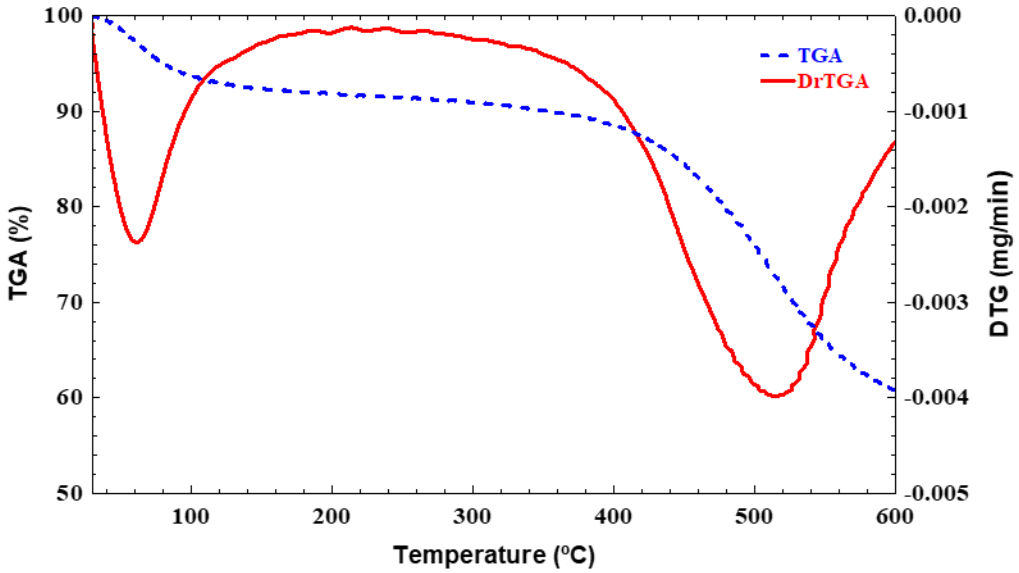

Fig. 3. Thermogravimetric (TGA) and derivative thermogravimetric (DTG) analysis of OP-AC

Between 150 and 400 °C, the TGA curve became notably stable, indicating the absence of major decomposition events. This thermal plateau is typical for fully carbonized lignocellulosic materials in which hemicellulose, cellulose, and other thermally labile components have been eliminated during activation (Raupp *et al.* 2021; Ramos *et al*. 2025). The lack of prominent DTG signals in this region confirms the formation of a robust aromatic carbon matrix (Grioui *et al*. 2023). The thermal stability within this intermediate temperature range highlights the structural integrity of OP-AC and its resistance to decomposition under moderate thermal conditions (Alouiz *et al*. 2024).

A significant degradation stage occurred above 400 °C, marked by a pronounced DTG peak. This mass loss is attributed to the thermal decomposition of oxygen-containing functional groups, such as phenolic, carboxylic, and lactonic moieties, as well as phosphorus-containing structures introduced during H_3PO_4 activation (Sadeek *et al*. 2020; Kiełbasa *et al*. 2022). These functional groups play an essential role in adsorption processes

and their decomposition at this stage aligns with the behavior of phosphoric acid ACs reported in the literature, which commonly exhibit major mass losses in the same temperature region due to the breakdown of linked organic and inorganic structures (Raupp *et al*. 2021; Alcazar-Ruiz *et al*. 2024; Alouiz *et al*. 2024).

Overall, the TGA/DTG analysis demonstrates that OP-AC had excellent thermal stability, low volatile content, and a highly carbonized aromatic framework. These features reflect the efficiency of H_3PO_4 activation in producing a stable microporous–mesoporous adsorbent. The observed thermal behavior is consistent with previously reported TGA profiles for different OP-AC by Raupp *et al*. (2021), Kiełbasa *et al*. (2022), Alouiz *et al*. (2024), and Alcazar-Ruiz *et al*. (2024). The combination of thermal resilience and well-developed porosity enhances the reusability and regeneration potential of OP-AC, making it a promising low-cost adsorbent for environmental applications, including the treatment of phenol-rich OMWW.

SEM Analysis of OP-AC

The SEM micrographs in Fig. 4 reveal the characteristic surface morphology of the OP-AC, displaying a highly heterogeneous, fractured, and porous structure consistent with thermochemical activation using phosphoric acid. The surface appears densely populated with irregular cavities, fissures, and granular aggregates, indicating the development of a multi-scale pore network that includes macropores, mesopores, and micropores, as detected by Chafi *et al*. (2025). Such morphological diversity is essential for adsorption processes, as macropores enhance diffusion and transport, while mesopores and micropores provide the active adsorption sites responsible for phenolic uptake (Ozcan *et al*. 2024).

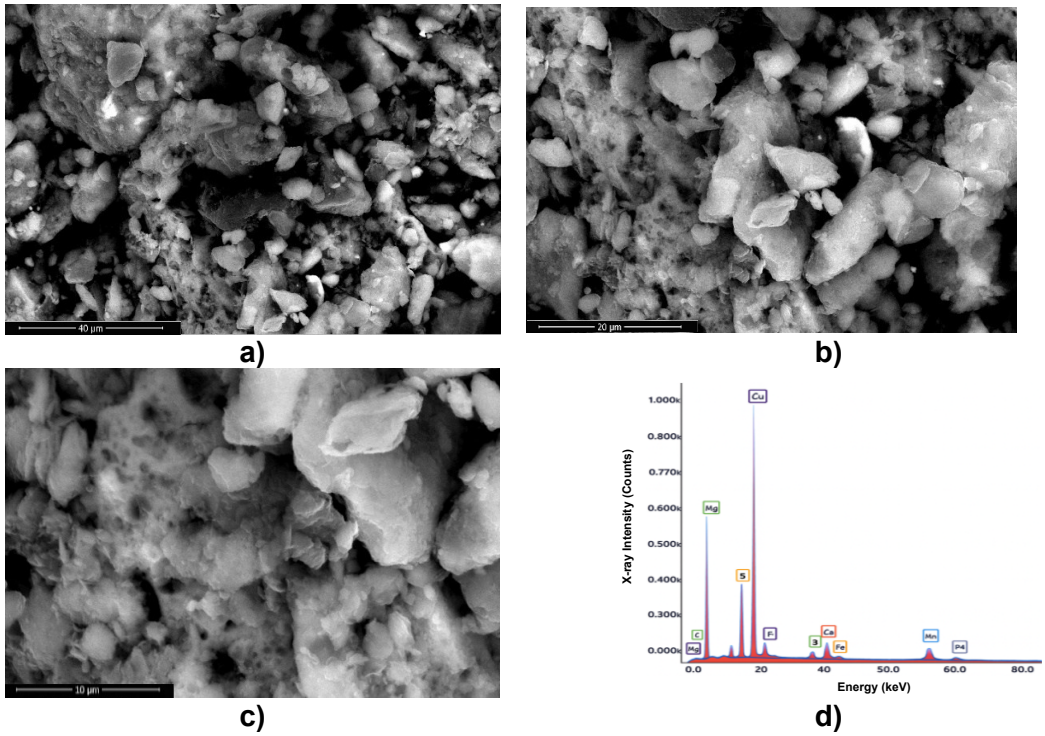

Fig. 4. SEM observations of the morphological characteristics of OP-AC at different magnifications a) 40 µm, b) 20 µm, c) 10 µm, and d) element composition *via* EDX analysis

The images further show numerous plate-like and rock-shaped carbon fragments, a typical feature of lignocellulosic biomass carbonized under acid activation. These fractured regions arise from the degradation and dehydration of hemicellulose, cellulose, and lignin, coupled with the formation of phosphate-cross-linked carbon matrices (Deniz *et al*. 2022). This confirms the structural integrity of the precursor and demonstrates the effectiveness of H_3PO_4 in promoting pore development through swelling, bond cleavage, and volatile release (Metyouy *et al*. 2024).

At the magnifications used, the SEM micrographs highlight well-defined cavities and interconnected porous channels, supporting the high iodine value (948 mg/g) and the substantial surface area expected for OP-AC. The presence of bright mineral inclusions dispersed across the carbon surface suggests the retention of inorganic elements such as Al, Ca, Fe, Si, P, Ti, Sr, and Zn, forming corresponding metal oxides (*e.g.*, SiO_2, CaO, FeO, Al_2O_3) (Chafi *et al*. 2025). These inorganic phases contribute additional adsorption functionality by offering ion-exchange, catalytic, or complexation sites, especially relevant for phenolic species in OMWW (Alouiz *et al*. 2025b).

Overall, the SEM features align closely with reported morphologies of AC derived from olive mill residues and other agricultural biomasses. Previous studies have similarly documented rough, cracked, and porous architectures for H_3PO_4-activated pomace, grape marc, and date pits, attributing the enhanced adsorption efficiency to their heterogeneous pore structure and residual inorganic constituents (Raupp *et al*. 2021; Bougheriou and Ghoualem 2023; Alouiz *et al*. 2025b). The high pore density and mineral heterogeneity observed here confirm that the synthesized OP-AC exhibits advanced structural characteristics that support efficient OMWW detoxification, particularly for phenolic removal.

Adsorption Kinetics

Adsorption equilibrium time for phenolic removal from OMWW using OP-AC was evaluated under batch conditions. Figure 5 illustrates the kinetic behavior of phenol adsorption onto OP-AC and provides visual confirmation of the trends quantified in Table 2. The experimental kinetic curve shows a steep adsorption phase during the first 20 to 30 minutes, driven by rapid film-diffusion and abundant external adsorption sites, which matches the relatively high predicted equilibrium capacities obtained from the kinetic models. The pseudo-first-order model captured this early adsorption behavior reasonably well, as indicated by its low deviation (2.02%) and accurate prediction of q_e (42.0 mg/g). Its alignment with the initial portion of the curve reflects the dominance of fast physisorption processes occurring on the external surface, consistent with the initial steep slope.

The pseudo-second-order model, which best matched the full experimental curve trajectory, particularly as equilibrium approached, also agrees with the multistage behavior visible in Fig. 5. Although its deviation (4.89%) was slightly higher, its curve followed the experimental data more closely during later stages of adsorption, reflecting the increasing contribution of slower surface-complex formation. This corresponds with the flattening of the kinetic curve as intraparticle transport becomes the rate-limiting step. FTIR results, which confirmed the presence of oxygenated functional groups, support this mixed mechanism involving both rapid physical adsorption and slower chemical interactions.

The intraparticle diffusion model, represented in Fig. 5 by a non-linear curve, only matched a portion of the experimental trend, highlighting that internal pore diffusion is not the sole controlling mechanism. The non-zero intercept (C = 20.49 mg/g) and high

deviation (14.47%) confirm the significance of boundary-layer resistance early on, consistent with the sharp initial adsorption observed in the kinetic plot. The later-stage deviation between the intraparticle diffusion line and the experimental curve aligns with OP-AC's heterogeneous macroporous–mesoporous–microporous structure observed in SEM images.

Overall, combining the graphical interpretation of Fig. 5 with the quantitative model assessment in Table 2 shows that phenol adsorption onto OP-AC was governed by a dual-stage mechanism: an initial rapid uptake controlled by external surface diffusion, followed by slower intraparticle diffusion and binding surface. The pseudo-second-order model best represents the overall adsorption behavior, while the pseudo-first-order model more closely describes the initial phase dominated by physisorption. These findings are fully consistent with adsorption mechanisms reported for lignocellulosic ACs used in OMWW and other phenolic-rich agro-industrial effluents (Hubbe 2022; Hubbe *et al.* 2019; Raupp *et al*. 2021; Bougheriou and Ghoualem 2023; Metyouy *et al*. 2024; Alouiz *et al*. 2025b).

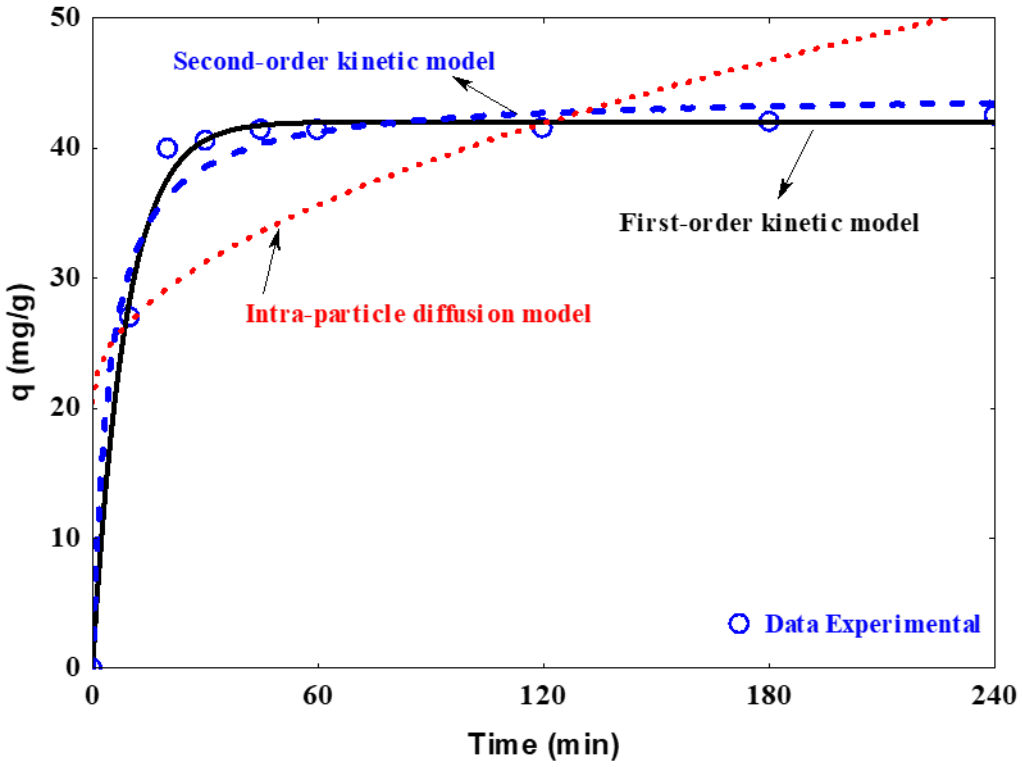

Fig. 5. Adsorption kinetics of phenolics onto OP-AC, C_i = 500 mg/L, T = 20 ºC, and pH = 4.50

Table 2. Data of the Adsorption Kinetics of Phenolics onto OP-AC the Different Models

q_e (exp.) (mg/g)	1st Order			2nd Order			Intraparticle Diffusion		
	q_e (pred.) (mg/g)	k_1 (1/min)	%D	q_e (pred.) (mg/g)	k_2 (g/mg/min)	%D	K_{id} (mg/g/min)	C (mg/g)	%D
42.04	42.04	0.11	2.02	44.29	0.01	4.89	1.96	20.49	14.47

Adsorption Isotherms

Figure 6 illustrates the adsorption isotherm of phenolic compounds from OMWW onto OP-AC, while Table 3 provides the corresponding parameters obtained from fitting the experimental data to the Langmuir, Freundlich, and Prausnitz–Radke isotherm models. Together, these results give a comprehensive understanding of the adsorption mechanism, surface heterogeneity, and affinity characteristics of the OP-AC surface. The experimental adsorption curve shows a steep initial rise at low equilibrium concentrations (C_e), indicating strong affinity and abundant available active sites on OP-AC (Abu-Dalo *et al*. 2023; Metyouy *et al*. 2024). As C_e increases, the curve gradually approaches a plateau, reflecting progressive saturation of higher-energy sites. This general behavior is consistent with porous carbonaceous adsorbents where multilayer adsorption coexists with monolayer surface interactions (Chafi *et al*. 2025; Qu *et al*. 2025).

The Langmuir model fits reasonably well at low phenol concentrations but deviates at higher C_e values, underestimating the adsorption capacity. This is reflected in the Langmuir parameters in Table 3, where the predicted maximum adsorption capacity (X_m = 874 mg/g) indicates strong monolayer adsorption potential, but the model exhibits a relatively high deviation (%D = 11.59%). The high BX_m value (60.5 L/g) indicates a strong initial affinity between phenolics and OP-AC; however, the deviation suggests that adsorption does not occur solely on homogeneous sites, and the carbon surface cannot be described by a purely monolayer mechanism.

The Freundlich model exhibits the best alignment with experimental data across the entire C_e range. Table 3 confirms this through the lowest deviation among all models (%D = 7.45%). The Freundlich constant (K_F = 15.6 L/g) indicates a high adsorption capacity, while the value of $1/n_F$ = 0.25 demonstrates strong surface heterogeneity and favorable multilayer adsorption; similar findings were found by Metyouy *et al.* (2024). The good agreement between the Freundlich model and the experimental data suggests that the adsorption process can be described by an empirical multilayer adsorption behavior, potentially supported by π–π interactions and hydrogen bonding with oxygenated functional groups identified *via* FTIR (Raupp *et al*. 2021; Alouiz *et al*. 2025b).

Table 3. Calculated Adsorption Parameters Obtained by Applying the Different Isotherm Models

Isotherm Model	Constants		Values
Langmuir	X_m [(a)]	(mg/g)	874.24
	B [(b)]	(L/mg)	0.07
	BX_m [(c)]	(L/g)	60.49
	%D		11.59
Freundlich	K_F [(d)]	(L/g)	15.57
	$1/n_F$ [(e)]		0.25
	%D		7.45
Prausnitz–Radke	a [(f)]	(L/g)	73205.00
	b [(g)]	(L^{β}/mg^{β})	4671.29
	β [(h)]		0.75
	%D		7.48

Note: [(a)] X_m: Capacity of adsorption (mg/g); [(b)] B: Constant (L/mg); [(c)] BX_m: Adsorbent–adsorbate relative affinity (L/g); [(d)] K_F: Relative capacity for adsorption (L/g); [(e)] $1/n_F$: Sorption intensity or surface heterogeneity; [(f)] Constant (L/g); [(g)] Constant (L^{β}/mg^{β}); and [(h)] Constant.

The Prausnitz–Radke model demonstrates an intermediate fit, capturing both the rapid initial uptake and the gradual approach to saturation. The parameters listed in Table

3 (a = 73200 L/g, b = 4670 L^{β}/mg^{β}, β = 0.75) reflect a hybrid adsorption mechanism incorporating both Langmuir-type monolayer behavior and Freundlich-type heterogeneity. The moderate deviation (%D = 7.48%) further supports this interpretation. This model's ability to bridge the two classical isotherms makes it particularly suitable for describing adsorption on structurally complex materials such as activated biomass carbons.

These findings are in agreement with previous studies by Ozcan *et al*. (2024) and Abu-Dalo *et al*. (2023), which show that lignocellulosic ACs exhibit mixed-mode adsorption, governed by both surface complexation and pore-diffusion phenomena. The combined interpretation of the isotherm curves and model parameters strongly supports the suitability of OP-AC as an efficient adsorbent for phenolic compounds in OMWW.

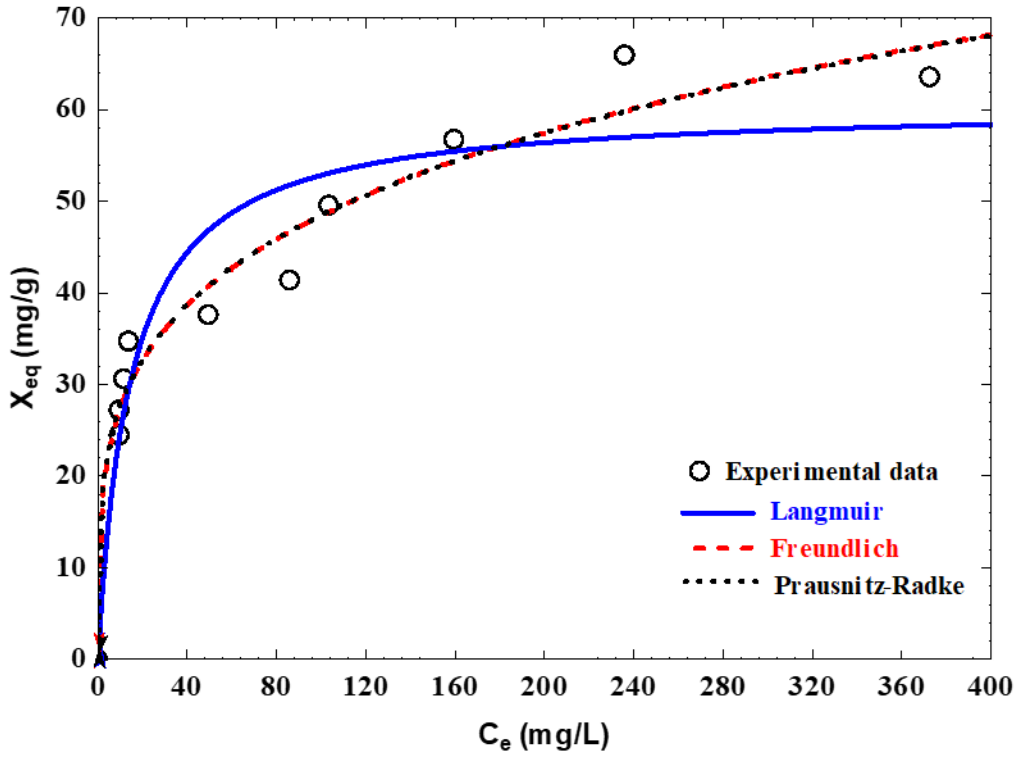

Fig. 6. Adsorption isotherm of phenolics onto OP-AC, C_i = 500 mg/L, T = 20 ºC, and pH = 4.50

Effect of Solution pH

Figure 7 indicates the effect of pH on the phenolic adsorption from OMWW onto OP-AC. The trend clearly demonstrates that pH is a dominant parameter governing adsorption performance since it simultaneously influence the surface charge of the OP-AC and the ionization state of phenolic molecules.

At strongly acidic conditions (pH 1 to 2), the adsorption capacity reaches its maximum, with q values corresponding to phenolic removal efficiencies of ≈79% to 80%. This high performance results from the extensive protonation of phenolic compounds, which remain in their neutral molecular (non-ionized) form, enhancing hydrophobic interactions, π–π stacking, and hydrogen bonding with the oxygen-containing functional groups. Additionally, the OP-AC surface may undergo protonation, which may influence adsorption behavior; however, the presence of positively charged groups is expected to be limited and pH-dependent (Grioui *et al*. 2023). This behavior aligns with the optimal pH values reported for phenolic adsorption onto lignocellulosic carbons, which confirmed that

acidic environments maximize sorption affinity (Raupp *et al*. 2021; Ozcan *et al*. 2024; Alouiz *et al*. 2025b).

As the pH increases toward neutrality (pH 4 to 8), the adsorption capacity sharply declines. This reduction originates changes in speciation, where carboxylic groups are deprotonated in this pH range, while phenolic groups remain largely non-ionized due to their higher pKa (~10), which increases their solubility and decreases their affinity for the carbon surface (Peeters *et al*. 2021). At the same time, OP-AC becomes less positively charged, reducing electrostatic and hydrogen-bond interactions. These combined effects result in markedly lower adsorption capacities, consistent with the minima observed around pH 6 to 8.

Interestingly, as the pH increased further into the alkaline region (pH 10 to 12), the adsorption capacity begins to rise again, although not reaching the acidic maximum. This secondary increase reflects the complex composition of OMWW, which contains a mixture of inorganic ions and trace metals. Under basic conditions, phenolic compounds are predominantly present as phenolate anions (pH > pKa ≈ 10), which can interact with embedded metal oxides (*e.g.*, FeO, Al_2O_3, CaO) detected by XRF, forming coordination complexes or undergoing surface precipitation. Such interactions explain the improved adsorption performance observed at high pH, despite the general expectation that phenolate ions exhibit lower affinity for carbon surfaces (Qu *et al*. 2025). Overall, Fig. 7 confirms that the adsorption behavior of phenolic compounds on OP-AC is strongly pH-dependent, with pH ≈ 2 representing the optimal operational condition for maximizing adsorption capacity and minimizing carbon consumption. Similar trends have also been reported by Raupp *et al*. (2021), Ozcan *et al*. (2024), and Alouiz *et al*. (2025b).

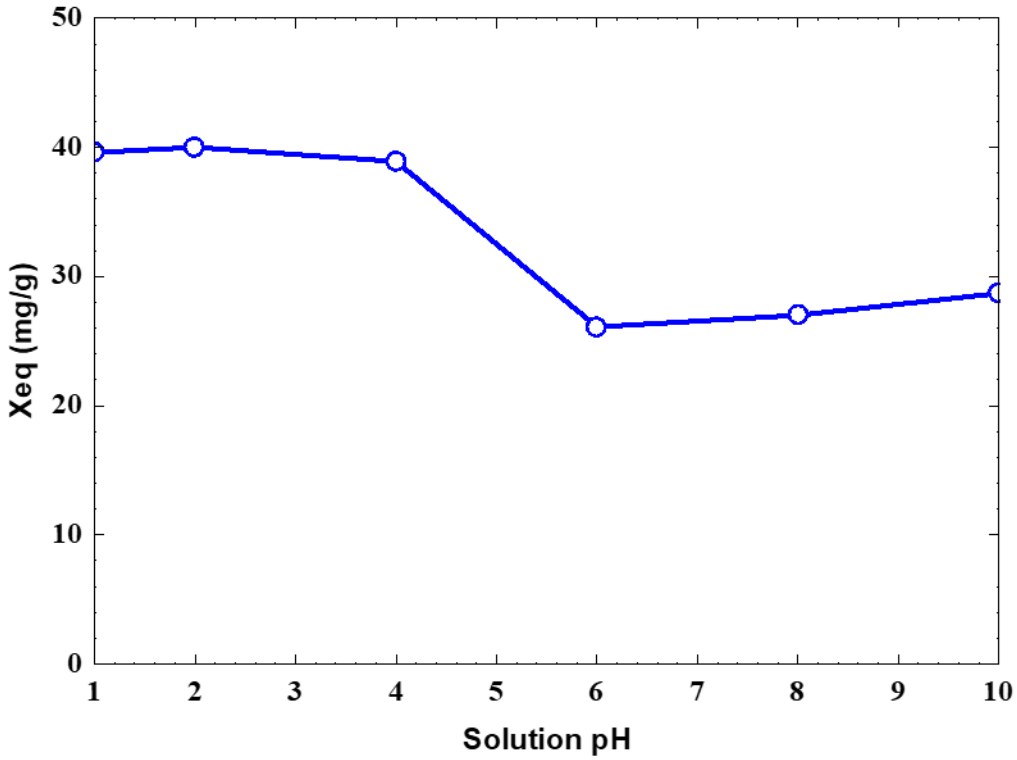

Fig. 7. Solution pH effect on the adsorption of phenolics onto OP-AC, C_i = 500 mg/L and T = 20 ºC

Effect of Temperature

Figure 8 a) indicates the temperature effect (20 to 100 °C) on the adsorption capacity of phenolic compounds from OMWW onto OP-AC. This wide temperature range was chosen to address both practical relevance and fundamental insights. From a practical standpoint, industrial wastewater is often discharged at temperatures reaching 100 °C, making these conditions pertinent when cooling is not cost-effective. From a fundamental perspective, the broad range allows for a thorough thermodynamic analysis, including the determination of activation energy. The trend provides clear evidence that adsorption efficiency was strongly and inversely dependent on temperature, confirming the exothermic nature of the adsorption process. At 20 to 30 °C, adsorption capacity was at its highest, corresponding to phenolic removal efficiencies of 78.2% to 80.0%. These temperatures favor physisorption mechanisms between phenolic molecules and oxygenated functional groups on OP-AC (Metyouy *et al*. 2024). This behavior confirms that ambient-temperature conditions are optimal for OMWW treatment, requiring no external heating and thus minimizing operational costs as reported by Ozcan *et al*. (2024).

As the temperature increased to 60 °C, the phenolic adsorption efficiency decreased to 57.4%. At this point, the heightened kinetic energy of phenolic molecules disrupted weak intermolecular forces, reducing their affinity with the carbon surface. A more dramatic decline occurred at 90 to 100 °C, where removal efficiencies dropped sharply to 31% and 20.6%, respectively. At these temperatures, adsorbed phenolic molecules gain enough energy to desorb from the carbon surface, and the structural water in OP-AC may undergo thermal changes that further limit adsorption. These observations confirm that increasing temperature shifted the equilibrium toward desorption, a hallmark of exothermic physisorption. Importantly, this thermal sensitivity is advantageous for adsorbent regeneration: the same elevated temperatures that reduce adsorption efficiency can be leveraged for thermal desorption, enabling OP-AC reuse (Bougheriou and Ghoualem 2023; Elamraoui *et al*. 2025).

Figure 8 b) illustrates the Van't Hoff relationship for the adsorption of phenolic compounds onto OP-AC, where the linear dependence of $\ln K_c$ on $1/T$ confirms the suitability of the Van't Hoff model and reflects classical thermodynamic behavior for this adsorption system, based on Eqs. 10 and 11. The thermodynamic parameters derived from Table 4 further validate these trends. The negative enthalpy change ($\Delta H° = -11.7$ kJ/mol) demonstrates that the adsorption process was exothermic, consistent with the experimentally observed decline in adsorption efficiency at higher temperatures and the predominance of physisorption mechanisms such as π–π interactions, hydrogen bonding, and Van der Waals forces (Ozcan *et al*. 2024; Elamraoui *et al*. 2025). Likewise, the strongly negative entropy value ($\Delta S° = -4380$ kJ/mol·K) reflects a substantial decrease in randomness at the solid–liquid interface, suggesting that phenolic molecules become more ordered upon attachment to the OP-AC surface, a behavior typical of lignocellulosic ACs with abundant micro- and mesopores (Metyouy *et al*. 2024).

The Gibbs free energy values ($\Delta G° < 0$ across all temperatures), according to Eqs. 12 and 13, confirm that the adsorption process was spontaneous, although the decrease in $\Delta G°$ magnitude temperature rises indicates reduced favorability at increased temperatures, which corroborates the exothermic behavior of the interaction (Abu-Dalo *et al*. 2023; Alouiz *et al*. 2025b). The alignment between the linear Van't Hoff plot and the calculated thermodynamic data collectively supports a mechanism dominated by weak physical forces with minor contributions from surface chemical interactions. These results corroborate previous findings from kinetic, pH, and temperature studies, emphasizing that OP-AC

exhibits optimal adsorption performance at ambient temperatures (20 to 30 °C) and is highly suitable for the sustainable treatment of phenol-rich OMWW under low-energy conditions,

$$\ln K_c = \frac{\Delta S^0}{R} - \frac{\Delta H^0}{RT} \quad (10)$$

$$\ln K_c = \frac{q_e}{C_e} \quad (11)$$

$$\Delta G^0 = -RT \ln K_c \quad (12)$$

$$\Delta G^0 = \Delta H^0 - T\Delta S^0 \quad (13)$$

where, K_c, R, and T (K) are the constants of thermodynamic equilibrium (L/g), universal gas (8.314 J/mol/K), and solution absolute temperature, respectively. From Eq. 10, graphing $\ln K_c$ *versus* $1/T$ yielded a linear graph (Fig. 8b). Table 4 indicated the ΔH_o and ΔS_o (calculated from slope and intercept). The negative ΔH_o in Table 4 indicated exothermic adsorption. The spontaneous adsorption of phenol on Carbon C is indicated by the negative value of ΔG^o, and the decrease in $\Delta G°$ values with rising temperature indicates that the adsorption process became less favorable at higher temperatures.

Table 4. Thermodynamic Parameters for the Adsorption of Phenolics onto OP-AC

Temperature (K)	lnK_c	ΔG^o (kJ/mol)	ΔH^o (kJ/mol)	ΔS^o (kJ/mol.K)
293	0.36	-960.32	-11.6596	-4376.57
303	0.40	-843.73		
333	0.13	-493.94		
363	0.04	-144.15		
373	0.03	-27.56		

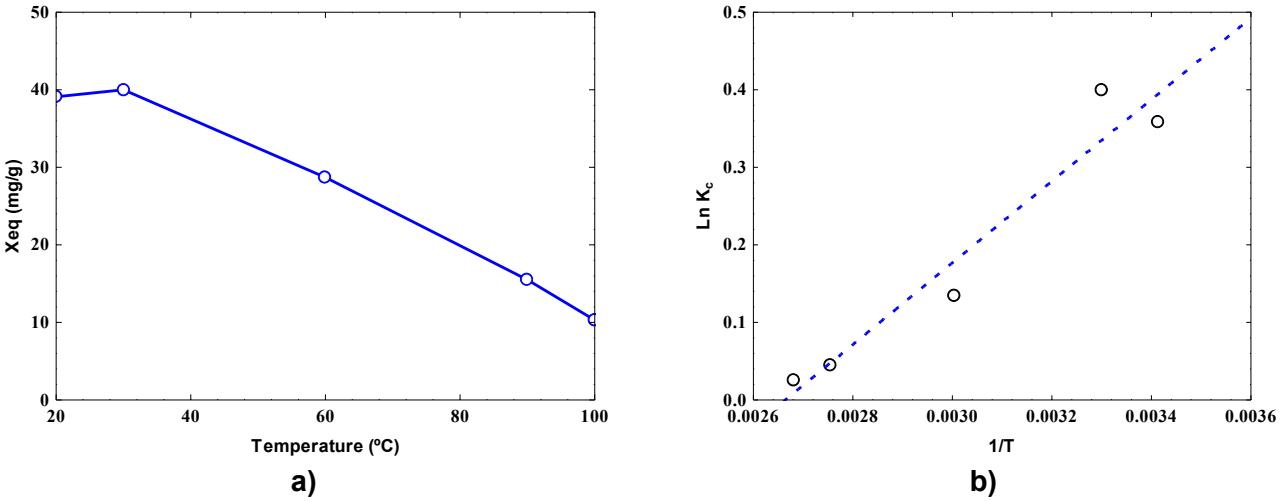

Fig. 8. a) Influence of temperature and b) Van't Hoff plot on the adsorption of phenolics onto OP-AC, C_i = 500 mg/L and pH =4.5

Integrated Treatment Process

The results presented in Table 5 and illustrated graphically in Fig. 9 demonstrate the effectiveness of the integrated treatment system, consisting of T1 followed by T2, in improving the physicochemical characteristics of OMWW. The crude OMWW exhibited excessive levels of TS (90.3 g/L), high EC (7.13 dS/m), and large organic loads, including TOC (27.1 g/L), COD (111 g/L), and BOD (61.3 g/L). Similar results were reported by El Shahawy *et al*. (2021), Elamraoui *et al*. (2025), Alouiz *et al*. (2025a), and Sarti *et al*. (2023). These values indicate intense salinity, strong recalcitrance, and severe biodegradability challenges, making crude OMWW unsuitable for discharge or reuse (Awadallah *et al*. 2023; Benaddi *et al*. 2023).

These values far exceed national and international guidelines; for example, the MWE maximum permissible limit for BOD in treated effluent is 40 g/L, while the FAO limit for EC in irrigation water is 3 dS/m. Additionally, the crude wastewater contained exceptionally high levels of total phenolics (5.00 g/L), surpassing the MWE allowable limit of 2.00 g/L, and enriched concentrations of monovalent ions (Na^+, K^+) and heavy metals (Fe^{3+}, Cu^{2+}, Mn^{2+}, Zn^{2+}), several of which exceeded FAO/MWE standards as reported by Khdair and Abu-Rumman (2020), Elamraoui *et al*. (2025), and Khalil *et al*. (2021). These characteristics confirm the necessity of a robust, multi-stage treatment approach.

The treatment T1 led to substantial reductions in suspended matter, organic load, and metal concentrations, primarily through coagulation, flocculation, and sedimentation mechanisms. TS decreased by 47.6%, and EC dropped by nearly 30%, reflecting the removal of colloids, tannin–metal complexes, and precipitated salts. Organic parameters such as TOC, COD, and BOD showed moderate reduction (29% to 35%), indicating that acid precipitation can destabilize and partially remove particulate and colloidal organic matter but cannot fully eliminate dissolved organics. Phenolic compounds decreased by 28.8%, demonstrating that polyphenols undergo partial protonation-induced coagulation at low pH. The removal of monovalent ions such as K^+ (55.2%) and Na^+ (54.4%) suggests that acidification enhances aggregation with dissolved organic matter and promotes precipitation of some inorganic species. Transition metals (Fe^{3+}, Cu^{2+}, Mn^{2+}, Zn^{2+}) exhibited removal efficiencies between 40% and 54%, aligning with their strong tendency to form insoluble complexes under acidic conditions. These findings align with those reported by earlier studies (Alrowais *et al*. 2023c; Benaddi *et al*. 2023).

The treatment T2 markedly enhanced removal efficiency across all parameters. The adsorption stage reduced TS by an additional 40.1%, achieving a final removal of 87.7%, consistent with the AC's ability to capture fine colloids and dissolved macromolecules (Alouiz *et al*. 2025a). EC removal increased dramatically (61.8%), yielding a total reduction of 91.7%, which reflects the strong affinity of OP-AC for ionic species and supports its capacity for salinity reduction, a crucial factor for agricultural reuse. Organic pollutants were significantly reduced in this step: TOC decreased by 51.2%, COD by 54.1%, and BOD by 56.0%, confirming the efficiency of the microporous–mesoporous carbon matrix and its functional groups (carboxylic, phenolic, lactonic) in adsorbing recalcitrant organics and improving effluent biodegradability (El-Shatoury *et al.* 2014; Alrowais *et al.* 2024; Alouiz *et al.* 2025a).

The most remarkable improvement occurred in the removal of total phenolic compounds, where T2 achieved 70.4% removal after acidification. When combined, the integrated system achieved a near-complete removal of 99.2%, reducing phenolic concentration from 5.0 g/L to only 0.04 g/L. This highlights the strong adsorption capacity

of OP-AC for phenolics, consistent with its high iodine value and oxygenated functional group composition identified earlier (Abu-Dalo *et al*. 2021).

The OP-AC developed in this study exhibited superior performance compared with previously reported biomass-derived activated carbons for phenolic removal. It showed a high iodine value (948 mg/g), indicating well-developed adsorption sites and strong affinity toward phenolic compounds. Most importantly, the integrated OP-AC system achieved a removal efficiency exceeding 99%, which is significantly higher than the 70 to 90% range commonly reported for olive-pomace-, olive-residue-, and other biomass-derived activated carbons (Abu-Dalo *et al*. 2021; Raupp *et al.* 2021; Bougheriou and Ghoualem 2023; Djeziri *et al.* 2023). This enhanced performance can be attributed to both the effective adsorption properties of OP-AC and the integration of adsorption with acid precipitation in the proposed treatment system, highlighting its potential as a highly efficient and sustainable approach for OMWW treatment.

For inorganic contaminants, T2 contributed significantly to the removal of metals and nutrients. Sodium and potassium levels were further reduced by 36.9% and 25.1%, respectively, achieving final removal of 91.2% (Na^+) and 80.4% (K^+), demonstrating reduced salinity hazards. Metals exhibited high T2 removal efficiencies: Fe^{3+} (34.3%), Cu^{2+} (44.2%), Mn^{2+} (44.3%), and Zn^{2+} (47.5%), with total removals exceeding 85% to 93%. This behavior is attributed to surface complexation and ion exchange with the mineral oxides (Al_2O_3, FeO, CaO, P_2O_5) detected in OP-AC, which facilitate metal fixation (Alouiz *et al.* 2025a).

When the effects of both T1 and T2 were combined, the integrated treatment system exhibited outstanding performance, with total removal efficiencies exceeding 85% for TS, COD, BOD, TOC, and EC. Figure 9 highlights this cumulative effect through the combined bars representing T1 + T2. The integrated removal of phenolics reached 99.2%, reducing their concentration from 5.00 g/L to just 0.039 g/L, which is well below the MWE standard of 2.00 g/L. Likewise, EC decreased by 91.7%, achieving a final value of 0.59 dS/m, which is comfortably within the FAO irrigation guideline (<3 dS/m). Similar improvements were achieved for metals: Fe^{3+} decreased from 4.43 to 0.50 mg/L, Cu^{2+} from 0.86 to 0.12 mg/L, Mn^{2+} from 0.61 to 0.04 mg/L, and Zn^{2+} from 1.18 to 0.15 mg/L. All final concentrations fell below both FAO and MWE limits, confirming the potential of the treated effluent for environmentally safe reuse.

Overall, the combined insights from Table 5 and Fig. 9 confirm that the sequential T1–T2 system was exceptionally capable of significantly reducing the organic constituents, inorganic, and phenolic load of OMWW. The process not only aligned with but surpassed regulatory benchmarks for irrigation and discharge quality. The complementary mechanisms of acid precipitation (colloid destabilization and partial ion removal) followed by OP-AC adsorption (strong surface binding and pore diffusion) resulted in a highly purified effluent suitable for agricultural applications, supporting sustainable wastewater management and circular economy principles through the valorization of OP-AC.

Table 5. Integrated Acid Precipitation (T1, pH 2.60, and 30 °C) and OP-AC Adsorption (T2, pH 2.00 and 30 °C) for OMWW Treatment

Parameter	OMWW (Mean ± SD)	T1 (Mean ± SD)	T2 (Mean ± SD)	T1+T2 Removal (%)	Standards	
					(MWE 2006)	(FAO 1985)
TS (g/L)	90.33 ± 3.51	47.33 ± 5.51	11.13 ± 0.36	87.68	2.54	2.00
EC (dS/m)	7.13 ± 0.19	5.00 ± 0.30	0.59 ± 0.05	91.73	--	3.00
TOC (g/L)	27.13 ± 3.80	17.67 ± 2.08	3.79 ± 0.26	86.03	--	--
COD (g/L)	111.33 ± 2.52	76.67 ± 7.64	16.46 ± 0.65	85.22	--	--
BOD (g/L)	61.26 ± 2.75	43.33 ± 2.52	9.00 ± 0.36	85.31	40.00	--
TPh (g/L)	5.00 ± 0.55	3.56 ± 0.40	0.04 ± 0.00	99.22	2.00	--
K^+ (g/L)	2.19 ± 0.26	0.98 ± 0.06	0.43 ± 0.31	80.37	--	--
Na^+ (g/L)	3.77 ± 0.21	1.72 ± 0.09	0.33 ± 0.04	91.25	--	--
Fe^{3+} (mg/L)	4.43 ± 0.95	2.02 ± 0.08	0.50 ± 0.06	88.71	5.00	5.00
Cu^{2+} (mg/L)	0.86 ± 0.06	0.50 ± 0.03	0.12 ± 0.02	86.05	0.40	0.20
Mn^{2+} (mg/L)	0.61 ± 0.05	0.31 ± 0.03	0.04 ± 0.01	93.44	0.20	0.20
Zn^{2+} (mg/L)	1.18 ± 0.17	0.71 ± 0.03	0.15 ± 0.02	87.29	4.00	2.00

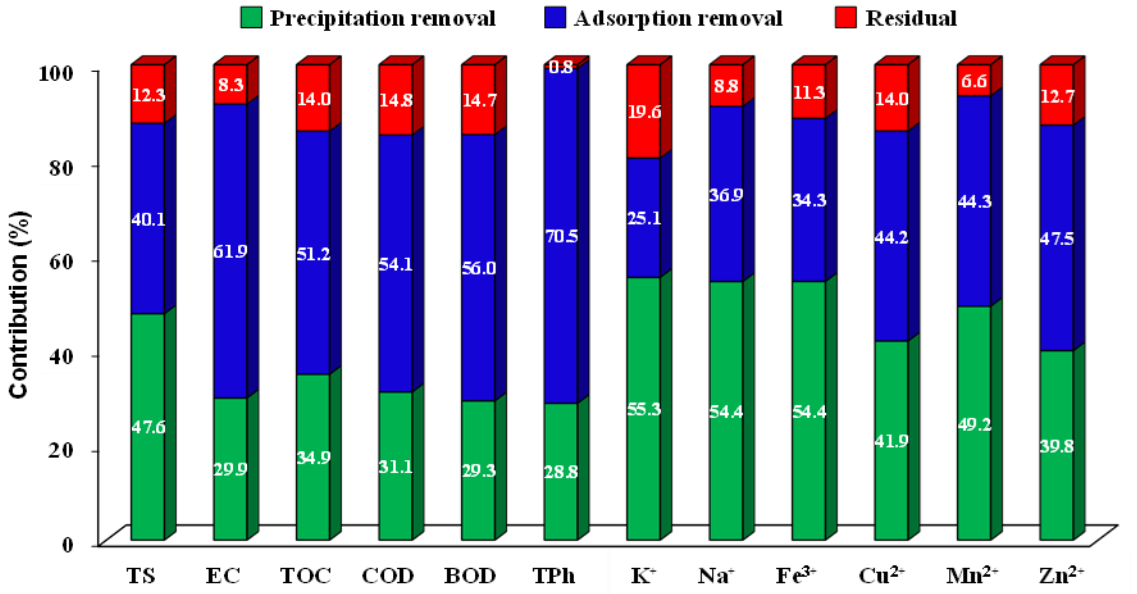

Fig. 9. Removal efficiency and treatment contribution of acid precipitation (T1, pH 2.60, and 30 °C) and OP-AC adsorption (T2, pH 2.00 and 30 °C) for OMWW parameters

Economic Study

Cost structure of OP-AC production and OMWW treatment

The economic analysis begins with the estimation of costs associated with the production of OP-AC and its application in the two-stage OMWW treatment system. OP is assumed to be available on-site at no purchase cost. Converting 1000 kg of dry OP into OP-AC yields approximately 300 kg, at a total production cost of 1,950 SAR, corresponding to 6.5 SAR/kg. Table 6 consolidates both OP-AC production costs and the

baseline (unoptimized) treatment cost per cubic meter of OMWW. Under conservative operating conditions, a relatively high OP-AC dosage of 15 kg/m³ is applied, resulting in a total treatment cost of 101.25 SAR/m³, of which adsorption is the dominant contributor. For an annual OMWW volume of 1000 m³, this corresponds to a treatment expenditure of 101,250 SAR/year.

Table 6. Consolidated Cost Structure for OP-AC Production and OMWW Treatment (SAR)

Category	Item	Cost	References
OP-AC Production (300 kg)	Pomace drying	375	(MARAFIQ 2025; SERA 2025)
	H_3PO_4 activation	937.5	(Yahya *et al*. 2015)
	Pyrolysis energy	150	(Manyà 2012)
	Washing & drying	100	(MARAFIQ 2025; SERA 2025).
	Labor	200	(Samarin and Al-Asfour 2023)
	Maintenance & depreciation	187.5	(Manyà 2012; Yahya *et al*. 2015)
	Total OP-AC production cost	**1,950**	
	Unit cost of OP-AC	**6.5 SAR/kg**	
OMWW Treatment (unoptimized)	T1: Acid precipitation	1.875 SAR/m³	(Alrowais *et al*. 2023c)
	T2: OP-AC adsorption (15 kg/m³)	99.375 SAR/m³	(Ahmed and Hameed 2020)
	Total treatment cost	**101.25 SAR/m³**	

Annual Economic Benefits and Baseline Balance

Although the direct treatment cost is high in the unoptimized scenario, the system generates substantial indirect economic value by avoiding disposal fees, regulatory penalties, and freshwater consumption. These benefits are summarized together with the annual cost balance in Table 7. For a facility treating 1000 m³ OMWW/year, total yearly benefits amount to approximately 78,094 SAR, dominated by avoided OMWW disposal costs and the reuse of treated water for irrigation. However, when compared with total annual costs (103,200 SAR, including OP-AC production and treatment), the system operates at a yearly net loss of 28,106 SAR in its unoptimized form (Manyà 2012; MARAFIQ 2025; SERA 2025).

Table 7. Annual Economic Benefits and Balance (unoptimized scenario, SAR/year)

Category	Description	Value
Benefits	Avoided OMWW disposal	37,500
	Avoided pomace disposal	93.75
	Avoided pollution fines	12,500
	Value of treated irrigation water	25,000
	Value of produced OP-AC	3,000
	Total annual benefits (A)	**78,093.75**
Costs	OP-AC production	−1,950
	OMWW treatment (1000 m³ × 101.25)	−101,250
	Total annual costs (B)	**−103,200**
Net balance (A − B)		**−28,106.25**

Optimization, Profitability, and Overall Economic Performance

Because OP-AC consumption represents the dominant cost driver, economic optimization focused on reducing adsorbent dosage and enabling material reuse. By lowering the OP-AC dosage to 5 kg/m³ and regenerating the adsorbent for five reuse cycles, the effective OP-AC cost decreases to 1.3 SAR/kg per use. Under these conditions, the total treatment cost is reduced to 10.25 SAR/m³, corresponding to an annual treatment cost of 10,250 SAR.

Table 8 integrates the optimized cost structure, revised annual balance, and additional revenue from selling surplus OP-AC. In the optimized configuration, total annual costs decline to 12,200 SAR, while benefits remain unchanged, resulting in a net annual profit of 62,894 SAR. If only half of the OMWW volume is treated on-site, surplus OP-AC sales can further increase the profit to approximately 64,394 SAR/year.

Table 8. Optimized Economic Performance and Profitability Summary (SAR)

Item	Value	Annual Cost (1000 m³)
Optimized treatment cost	10.25 SAR/m³	103,200
Annual treatment cost (1000 m³)	10,250	12,200
OP-AC production cost	1,950	12,200
Total annual costs (optimized)	**12,200**	
Total annual benefits	75,093.75	
Net annual profit (optimized)	**62,893.75**	
Additional revenue from surplus OP-AC	1,500	
Total annual profit (with OP-AC sales)	**64,393.75**	

As shown in Table 9, the unoptimized scenario results in a substantial annual loss, primarily due to the high consumption of OP-AC, which dominates operating expenses. Despite significant environmental and regulatory benefits, the high treatment cost (101.25 SAR/m³) prevents economic viability under conservative operating conditions.

In contrast, the optimized scenario, incorporating reduced OP-AC dosage and five regeneration–reuse cycles, decreased the treatment cost by approximately 90%, yielding a positive net annual profit of ~62,900 SAR. This clearly identifies adsorbent consumption and reuse efficiency as the dominant economic drivers of the system. Further improvement is achieved when surplus OP-AC is valorized through external sale, increasing total annual benefits and raising the net profit to ~64,400 SAR. This highlights the added value of integrating co-product recovery within the circular treatment framework.

Overall, the scenario comparison demonstrates that while the proposed system is not economically feasible without optimization, it becomes clearly profitable when operational parameters are optimized, confirming that circular valorization and material reuse are essential for translating environmental effectiveness into economic sustainability.

Table 9. Summary of Economic Performance under Different Operating Scenarios

Scenario	Treatment Cost (SAR/m³)	Annual Cost (1000 m³)	Annual Benefits (SAR)	Net Annual Result
Unoptimized	101.25	103,200	75,093.75	−28,106.25 (Loss)
Optimized (5× reuse, lower dose)	10.25	12,200	75,093.75	+62,893.75 (Profit)
Optimized + surplus OP-AC sale	10.25	12,200	76,593.75	+64,393.75 (Higher profit)

Economic Implications

The consolidated analysis demonstrates that the proposed two-stage OMWW treatment system is not economically viable without optimization but becomes clearly profitable when adsorbent reuse and dosage reduction are applied. For Saudi olive mills, the main economic driver is not water sales, but the conversion of environmental liability into regulatory compliance, water security, and circular resource valorization. This makes the optimized system both an environmentally and economically rational solution for olive-producing regions.

Recommendations and Future Work

Future research should focus on validating the integrated T1–T2 treatment system at pilot and industrial scales to assess its practical feasibility, operational stability, and the long-term performance of OP-AC through systematic assessment of its reusability over multiple adsorption–regeneration cycles using both thermal and chemical desorption methods. Studies should also explore the selective recovery of high-value phenolic fractions removed during acid precipitation and adsorption, enabling their potential reuse in food, pharmaceutical, and cosmetic applications. Hybrid treatment configurations, combining OP-AC with advanced oxidation processes, membrane filtration, or anaerobic digestion, should be evaluated to move toward zero-liquid-discharge goals. Material enhancement strategies, such as co-activation using different or mixed chemical agents, metal doping, or nano-scale modification, may further improve surface area, pore structure, and adsorption selectivity. Broader applicability of OP-AC should be examined by testing its efficiency in removing dyes, pharmaceuticals, pesticides, and heavy metals from diverse industrial wastewaters. Finally, comprehensive techno-economic assessments are recommended to determine production costs, resource efficiency, and the commercialization potential of large-scale OP-AC fabrication.

CONCLUSIONS

Based on the comprehensive research presented, this study successfully demonstrated an integrated and sustainable approach for managing olive oil industry waste streams through the valorization of olive pomace activated carbon (OP-AC) for effective detoxification of olive mill wastewater (OMWW).

1. The OP-AC exhibited exceptional textural properties, including high microporosity evidenced by an iodine value of 948 mg/g and a substantial activation yield of 61%.
2. The sequential treatment system combining acid precipitation and adsorption proved remarkably efficient, achieving near-complete removal of phenolic compounds

(99.2%) and significant reduction of organic load (85 to 86% for COD, BOD, TOC), salinity (91.7% for EC), and heavy metals (88 to 93% for Fe^{3+}, Cu^{2+}, Mn^{2+}, Zn^{2+}).

3. Optimization studies revealed that maximum adsorption efficiency occurred at solution pH (2.00 to 3.00) and ambient temperature (20 to 30°C). The experiment data showed the best fit with the pseudo-second-order kinetic model and the Freundlich isotherm, suggesting multilayer adsorption on heterogeneous surfaces governed primarily by physisorption. Most significantly, the treated effluent quality met international irrigation standards (FAO and MWE), confirming the process's practical applicability.
4. Process optimization through reduced OP-AC dosage and five-cycle adsorbent reuse lowers OMWW treatment costs by ~90% (from 101.25 to 10.25 SAR/m³), transforming an unprofitable system into a profitable one.
5. The optimized process yields a net annual profit of ~63,000 SAR per 1000 m³, driven mainly by avoided disposal costs, regulatory compliance, water reuse, and circular valorization of OP, making it highly suitable for water-scarce olive-producing regions.
6. This research presents a circular economic solution that simultaneously addresses both solid and liquid waste challenges in olive oil production, offering an environmentally sustainable, cost-effective, and scalable technology for industrial wastewater treatment while supporting resource recovery and water reuse in water-scarce regions.

ACKNOWLEDGMENTS

This work was funded by the Deanship of Graduate Studies and Scientific Research at Jouf University under grant No. (DGSSR-2025-FC-01035).

During the preparation of this manuscript, the authors used ChatGPT (OpenAI) to assist with language editing and improving the clarity and organization of the text. The authors reviewed and edited the content and take full responsibility for the scientific accuracy and integrity of the work.

REFERENCES CITED

Abd El-wahaab, B., El-Shwiniy, W. H., Alrowais, R., Nasef, B. M., and Said, N. (2025). "Adsorption of (Pb (II)) from contaminated water onto activated carbon: kinetics, isotherms, thermodynamics, and modeling by artificial intelligence," *Sustainability* 17(5), article 2131. https://doi.org/10.3390/su17052131

Abdel daiem, M. M., Sánchez-Polo, M., Rashed, A. S., Kamal, N., and Said, N. (2019). "Adsorption mechanism and modelling of hydrocarbon contaminants onto rice straw activated carbons," *Polish Journal of Chemical Technology* 21(4), 1-12. https://doi.org/10.2478/pjct-2019-0032

Abu-Dalo, M. A., Al-Rawashdeh, N. A. F., Almurabi, M., Abdelnabi, J., and Al Bawab, A. (2023). "Phenolic compounds removal from olive mill wastewater using the composite of activated carbon and copper-based metal-organic framework," *Materials* 16(3), article 1159. https://doi.org/10.3390/ma16031159

Abu-Dalo, M., Abdelnabi, J., and Bawab, A. Al. (2021). "Preparation of activated carbon derived from jordanian olive cake and functionalized with $Cu/Cu_2O/CuO$ for

adsorption of phenolic compounds from olive mill wastewater," *Materials* 14(21), artilce 6636. https://doi.org/10.3390/ma14216636

Abu-Dalo, M., Abu-Dalo, D., Halalsheh, M., and Al Bawab, A. (2024). "Olive mill wastewater treatment using vertical flow constructed wetlands (VFCWs)," *BMC Chemistry* 18(1), article 234. https://doi.org/10.1186/s13065-024-01348-3

Ahmed, M. J., and Hameed, B. H. (2020). "Insight into the co-pyrolysis of different blended feedstocks to biochar for the adsorption of organic and inorganic pollutants: A review," *Journal of Cleaner Production* 265, article 121762. https://doi.org/10.1016/j.jclepro.2020.121762

Alcazar-Ruiz, A., Maisano, S., Chiodo, V., Urbani, F., Dorado, F., and Sanchez-Silva, L. (2024). "Enhancing CO_2 capture performance through activation of olive pomace biochar: A comparative study of physical and chemical methods," *Sustainable Materials and Technologies* 42, article e01177. https://doi.org/10.1016/j.susmat.2024.e01177

Aljubiri, S. M., Younes, A. A. O., Alosaimi, E. H., Abdel-Daiem, M. M., Abdel-Salam, E. T., and El-Shwiniy, W. H. (2024a). "Efficient removal of phenol red dye from polluted water using sustainable low-cost sewage sludge activated carbon: Adsorption and reusability studies," *Molecules* 29(24), article 5865. https://doi.org/10.3390/molecules29245865

Aljubiri, S. M., Younes, A. A. O., Alosaimi, E. H., Abdel daiem, M. M., Abdel-salam, E. T., and El-Shwiniy, W. H. (2024b). "Recycling of sewage sludge: Synthesis and application of sludge-based activated carbon in the efficient removal of cadmium (II) and lead (II) from wastewater," *International Journal of Molecular Sciences* 25(18), article 9866. https://doi.org/10.3390/ijms25189866

Alouiz, I., Benhadj, M., Dahmane, E., Sennoune, M., Amarouch, M.-Y., and Mazouzi, D. (2024). "Elaboration of fibrous structured activated carbon from olive pomace via chemical activation and low-temperature pyrolysis," *Heliyon* 10(20), article e39996. https://doi.org/10.1016/j.heliyon.2024.e38886

Alouiz, I., Benhadj, M., Dahmane, E., Sennoune, M., Amarouch, M. Y., and Mazouzi, D. (2025a). "Elimination of olive mill wastewater polyphenols through an olive pomace-derived activated charcoal," *Moroccan Journal of Chemistry* 13(1), 133-144. https://doi.org/10.48317/IMIST.PRSM/morjchem-v13i1.48039

Alouiz, I., Benhadj, M., Harboul, K., Boukhris, M., Elmontassir, D., Sennoune, M., Amarouch, M. Y., and Mazouzi, D. (2025b). "Activated carbon from olive pomace for hexavalent chromium removal: synthesis, characterization, and adsorption mechanism analysis," *Scientific Reports* 15(1), article 18576. https://doi.org/10.1038/s41598-025-95278-2

Alrowais, R., Abdel daiem, M. M., Li, R., Maklad, M. A., Helmi, A. M., Nasef, B. M., and Said, N. (2023a). "Groundwater quality assessment for drinking and irrigation purposes at Al-Jouf area in KSA using artificial neural network, GIS, and multivariate statistical techniques," *Water* 15(16), article 2982. https://doi.org/10.3390/w15162982

Alrowais, R., Abdel daiem, M. M., Nasef, B. M., and Said, N. (2024). "Activated carbon fabricated from biomass for adsorption/bio-adsorption of 2, 4-D and MCPA: Kinetics, isotherms, and artificial neural network modeling," *Sustainability* 16(1), article 299. https://doi.org/10.3390/su16010299

Alrowais, R., Said, N., Bashir, M. T., Ghazy, A., Alwushayh, B., and Abdel daiem, M. M. (2023b). "Adsorption of diphenolic acid from contaminated water onto

commercial and prepared activated carbons from wheat straw," *Water* 15(3), article 555. https://doi.org/10.3390/w15030555

Alrowais, R., Yousef, R. S., Ahmed, O. konsowa, Mahmoud-Aly, M., Abdel daiem, M. M., and Said, N. (2023c). "Enhanced detoxification methods for the safe reuse of treated olive mill wastewater in irrigation," *Environmental Sciences Europe* 35(1), article 95. https://doi.org/10.1186/s12302-023-00797-2

Annab, H., Fiol, N., Villaescusa, I., and Essamri, A. (2019). "A proposal for the sustainable treatment and valorisation of olive mill wastes," *Journal of Environmental Chemical Engineering* 7(1), article 102803. https://doi.org/10.1016/j.jece.2018.11.047

Awadallah, R. Y., Mohamed, A. A., and Abdelhafez, A. (2023). "Evaluation of biologically treated olive mill wastewater for irrigation of pea plant," *Arab Universities Journal of Agricultural Sciences*, Ain Shams University, Faculty of Agriculture, 31(1), 51-62.

Ayadi, K., Meziane, M., Rouam, D., Bouziane, M. N., and El-Miloudi, K. (2022). "Olive mill wastewater for bioethanol production using immobilised cells," *Kemija u Industriji: Časopis Kemičara i Kemijskih Inženjera Hrvatske, Hrvatsko Društvo Kemijskih Inženjera i Tehnologa* 71(1–2), 21-28. DOI: 10.15255/KUI.2021.015

APHA (2005). *Standard Methods for the Examination of Water and Wastewater*, American Public Health Association (APHA): Washington, DC, USA, 21.

Bazzarelli, F., Poerio, T., Mazzei, R., D'Agostino, N., and Giorno, L. (2015). "Study of OMWWs suspended solids destabilization to improve membrane processes performance," *Separation and Purification Technology* 149, 183-189. https://doi.org/10.1016/j.seppur.2015.05.040

Benaddi, R., Osmane, A., Zidan, K., El Harfi, K., and Ouazzani, N. (2023). "A review on processes for olive mill waste water treatment," *Ecological Engineering and Environmental Technology* 24, 7. https://doi.org/10.12912/27197050/169876

Bottino, A., Capannelli, G., Comite, A., Costa, C., Firpo, R., Jezowska, A., and Pagliero, M. (2020). "Treatment of olive mill wastewater through integrated pressure-driven membrane processes," *Membranes* 10(11), article 334. https://doi.org/10.3390/membranes10110334

Bougheriou, F., and Ghoualem, H. (2023). "Synthesis and characterization of activated carbons from walnut shells to remove diclofenac," *Iranian Journal of Chemistry and Chemical Engineering* 42(9), 131. https://doi.org/10.30492/ijcce.2023.559588.5499

Chafi, S., Cuevas-Aranda, M., Martínez-Cartas, M. L., and Sánchez, S. (2025). "Production of bioadsorbents via low-temperature pyrolysis of exhausted olive pomace for the removal of methylene blue from aqueous media," *Molecules* 30(15) artilce 3254. https://doi.org/10.3390/molecules30153254

Dahdouh, A., Khay, I., Le Brech, Y., El Maakoul, A., and Bakhouya, M. (2023). "Olive oil industry: A review of waste stream composition, environmental impacts, and energy valorization paths," *Environmental Science and Pollution Research* 30(16), 45473-45497. https://doi.org/10.1007/s11356-023-25867-z

Dali, I., Abdelwahab, A. T., Aydi, A., Fares, N., Eladeb, A., Hamzaoui, M., Abderrabba, M., Abdelfattah, M. A., and Guetat, A. (2023). "Valorization of lyophilized olive mill wastewater: chemical and biochemical approaches," *Sustainability* 15(4), article 3360. https://doi.org/10.3390/su15043360

Deniz, F., Başgöz, Ö., Güler, Ö., and Mazmancı, M. A. (2022). "Characterization and dye adsorption effectiveness of activated carbon synthesized from olive pomace,"

Environmental Research and Technology 5(4), 369-379. https://doi.org/10.35208/ert.1163939

Di Giacomo, G., and Romano, P. (2022). "Evolution of the olive oil industry along the entire production chain and related waste management," *Energies* 15(2), article 465. https://doi.org/10.3390/en15020465

Dich, A., Abdelmoumene, W., Belyagoubi, L., Assadpour, E., Belyagoubi Benhammou, N., Zhang, F., and Jafari, S. M. (2025). "Olive oil wastewater: A comprehensive review on examination of toxicity, valorization strategies, composition, and modern management approaches," *Environmental Science and Pollution Research* 32, 6349-6379. https://doi.org/10.1007/s11356-025-36127-7

Djeziri, S., Taleb, Z., and Djellouli, H. M. (2023). "Kinetic study of adsorption of phenolic compounds from olive oil mill wastewater on activated carbon," *Acta Periodica Technologica* (54), 197-208. https://doi.org/10.2298/APT2354197D

El Shahawy, A., Ahmed, I. A., Nasr, M., Ragab, A. H., Al-Mhyawi, S. R., and Elamin, K. (2021). "Organic pollutants removal from olive mill wastewater using electrocoagulation process via central composite design (CCD)," *Water* 13(24), article 3522. https://doi.org/10.3390/w13243522

El-Shatoury, S., El-Baz, A., Abdel Daiem, M., and El-Monayeri, D. (2014). "Enhancing wastewater treatment by commercial and native microbial Inocula with factorial design," *Life Science Journal* 11(7), 736-742. https://doi.org/10.7537/marslsj110714.108

Elamraoui, S., Asdiou, N., El kaim Billah, R., El Achaby, M., Kounbach, S., Benhida, R., and Achak, M. (2025). "Unveiling the adsorptive potential of natural biopolymers for olive mill wastewater treatment: A synergistic approach using RSM-BBD, mixture design, kinetics, and mechanistic analysis," *International Journal of Molecular Sciences* 26(16), article 7738. https://doi.org/10.3390/ijms26167738

FAO. (1985). "Food and Agriculture Organization, Water Quality for Agriculture. Irrigation and Drainage Paper No. 29 Rev.1, Rome."

Foo, K. Y., and Hameed, B. H. (2010). "Insights into the modeling of adsorption isotherm systems," *Chemical Engineering Journal* 156(1), 2-10. https://doi.org/10.1016/j.cej.2009.09.013

Foti, P., Romeo, F. V, Russo, N., Pino, A., Vaccalluzzo, A., Caggia, C., and Randazzo, C. L. (2021). "Olive mill wastewater as renewable raw materials to generate high added-value ingredients for agro-food industries," *Applied Sciences* 11(16), article 7511. https://doi.org/10.3390/app11167511

Grioui, N., Elleuch, A., Halouani, K., and Li, Y. (2023). "Valorization of exhausted olive pomace for the production of a fuel for direct carbon fuel cell," *C* 9(1), 22. https://doi.org/10.3390/c9010022

Hecini, L., and Achour, S. (2014). "Coagulation-floculation au sulfate d'aluminium de composés organiques phénoliques et effet de sels de calcium et de magnésium," *Revue des Sciences de l'Eau* 27(3), 271-280. https://doi.org/10.7202/1027810ar

Hubbe, M. A., Azizian, S., and Douven, S. (2019). "Implications of apparent pseudo-second-order adsorption kinetics onto cellulosic materials. A review," *BioResources* 14(3), 7582-7626. https://doi.org/10.15376/biores.14.3.7582-7626

Hubbe, M. A. (2021). "Insisting upon meaningful results from adsorption experiments," *Separation & Purification Reviews* 51(2), 121-225, article ID LSPR 1888299. https://doi.org/10.1080/15422119.2021.1888299

IMARC. (2024). Saudi Arabia Olive Oil Market Size, Share, Trends and Forecast by

Type, Distribution Channel, Application, and Region, 2025-2033.
IOC. (2024). "World Market of Olive Oil and Table Olives," International Olive Council, https://www.internationaloliveoil.org/world-market-of-olive-oil-and-table-olives-data-from-december-2024/.
Jamrah, A., Al-Zghoul, T., Baarimah, A. O., and Al-Karablieh, E. (2024). "A bibliometric analysis of olive mill wastewater treatment methods from 1988 to 2023," *Case Studies in Chemical and Environmental Engineering* 9, article 100736. https://doi.org/10.1016/j.cscee.2024.100736
Jarboui, R., Sellami, F., Kharroubi, A., Gharsallah, N., and Ammar, E. (2008). "Olive mill wastewater stabilization in open-air ponds: Impact on clay–sandy soil," *Bioresource Technology* 99(16), 7699-7708. https://doi.org/10.1016/j.biortech.2008.01.074
Khalil, J., Habib, H., Alabboud, M., and Mohammed, S. (2021). "Olive mill wastewater effects on durum wheat crop attributes and soil microbial activities: A pilot study in Syria," *Energy, Ecology and Environment* 6, 469-477. https://doi.org/10.1007/s40974-021-00209-2
Khdair, A., and Abu-Rumman, G. (2020). "Sustainable environmental management and valorization options for olive mill byproducts in the Middle East and North Africa (MENA) region," *Processes* 8(6), article 671. https://doi.org/10.3390/pr8060671
Kiełbasa, K., Bayar, Ş., Varol, E. A., Sreńscek-Nazzal, J., Bosacka, M., and Michalkiewicz, B. (2022). "Thermochemical conversion of lignocellulosic biomass-olive pomace-into activated biocarbon for CO_2 adsorption," *Industrial Crops and Products* 187, article 115416. https://doi.org/10.1016/j.indcrop.2022.115416
Kurtoğlu, S., Uzundumlu, A. S., and Gövez, E. (2024). "Olive oil production forecasts for a macro perspective during 2024–2027," *Applied Fruit Science* 66(3), 1089-1100. https://doi.org/10.1007/s10341-024-01064-1
Manyà, J. J. (2012). "Pyrolysis for biochar purposes: a review to establish current knowledge gaps and research needs," *Environmental Science and Technology* 46(15), 7939-7954. https://doi.org/10.1021/es301029g
MARAFIQ. (2025). "High intensity electricity consumption tarif," Electricity Tariff, https://marafiq.com.sa/
Medina, M. B. (2011). "Simple and rapid method for the analysis of phenolic compounds in beverages and grains," *Journal of Agricultural and Food Chemistry* 59(5), 1565-1571. https://doi.org/10.1021/jf103711c
Metyouy, K., Benkirane, L., Sánchez, M. E., Cara-Jiménez, J., Plakas, K. V, and Chafik, T. (2024). "Valorization of agricultural olive waste as an activated carbon adsorbent for the remediation of water sources contaminated with pharmaceuticals," *Sustainable Chemistry for the Environment* 6, artilce 100110. https://doi.org/10.1016/j.scenv.2024.100110
Mohammad, A. H., Radovic, I., Ivanović, M., and Kijevčanin, M. (2022). "Adsorption of metformin on activated carbon produced from the water hyacinth biowaste using H_3PO_4 as a chemical activator," *Sustainability* 14(18), article 11144. https://doi.org/10.3390/su141811144
MWE. (2006). "Technical guidelines for the use of treated sanitary wastewater in irrigation for landscaping and agricultural irrigation," Ministry of Water and Electricity, Kingdom of Saudi Arabia.
Niaounakis, M., and Halvadakis, C. P. (2006). "Olive processing waste management: Literature review and patent survey," *Waste Management Series*, Elsevier.

https://www.sciencedirect.com/bookseries/waste-management-series/vol/5/suppl/C
Ouda, O. K. M. (2013). "Review of Saudi Arabia municipal water tariff," *World Environment* 3(2), 66-70. https://doi.org/10.5923/j.env.20130302.05
Okpara, O. G., Ogbeide, O. M., Nworu, J. N., Chukwuekeh, J. I., Igoche, S. A., Alichi, F. S., and Orinya, O. E. (2023). "Enhanced removal of Pb (II), Cd (II), and Zn (II) ions from aqueous solutions using EDTA-synthesized activated carbon derived from sawdust," *Open Access Library Journal* 10(9), 1-15. https://doi.org/10.4236/oalib.1110690
Ozcan, D. O., Hendekci, M. C., and Ovez, B. (2024). "Enhancing the adsorption capacity of organic and inorganic pollutants onto impregnated olive stone derived activated carbon," *Heliyon* 10(12), article e32792. https://doi.org/10.1016/j.heliyon.2024.e32792
Peeters, K., Miklavčič Višnjevec, A., Esakkimuthu, E. S., Schwarzkopf, M., and Tavzes, Č. (2021). "The valorisation of olive mill wastewater from Slovenian Istria by Fe_3O_4 particles to recover polyphenolic compounds for the chemical specialties sector," *Molecules* 26(22), article 6946. https://doi.org/10.3390/molecules26226946
Posadino, A. M., Cossu, A., Giordo, R., Piscopo, A., Abdel-Rahman, W. M., Piga, A., and Pintus, G. (2021). "Antioxidant properties of olive mill wastewater polyphenolic extracts on human endothelial and vascular smooth muscle cells," *Foods* 10(4), article 800. https://doi.org/10.3390/foods10040800
Qadir, M., Drechsel, P., Jiménez Cisneros, B., Kim, Y., Pramanik, A., Mehta, P., and Olaniyan, O. (2020). "Global and regional potential of wastewater as a water, nutrient and energy source," *Natural Resources Forum* 44, 40-51. https://doi.org/10.1111/1477-8947.12187
Qasim, S. R. (2017). *Wastewater Treatment Plants: Planning, Design, and Operation*, 2nd Edition, Routledge, Taylor & Francis. CRC press. https://doi.org/10.1201/9780203734209
Qu, D., Yu, Y., Zhu, M., Lei, C., Wang, B., Wang, X., and Zhou, X. (2025). "Investigating olive pomace activated carbon for degrading organic dyes in water," *Scientific Reports* 15(1), article 15062. https://doi.org/10.1038/s41598-025-97402-8
Ramos, P. B., Mamani, A., Sardella, M. F., Arencibia, A., Sanz, R., Sanz-Pérez, E. S., Bavio, M. A., and Erans, M. (2025). "Olive mill waste-derived activated carbon for CO_2 capture using realistic conditions," *Energy and Fuels* 39(11), 5442-5452. https://doi.org/10.1021/acs.energyfuels.4c04880
Raupp, Í. N., Valério Filho, A., Arim, A. L., Muniz, A. R. C., and da Rosa, G. S. (2021). "Development and characterization of activated carbon from olive pomace: Experimental design, kinetic and equilibrium studies in nimesulide adsorption," *Materials* 14(22), article 6820. https://doi.org/10.3390/ma14226820
Roque, M. de L., Botelho, C., and Barros, A. N. (2025). "From waste to resource: chemical characterization of olive oil industry by-products for sustainable applications," *Molecules* 30(15), article 3212. https://doi.org/10.3390/molecules30153212
Roig, A., Cayuela, M. L., and Sánchez-Monedero, M. A. (2006). "An overview on olive mill wastes and their valorisation methods," *Waste Management* 26(9), 960-969. https://doi.org/10.1016/j.wasman.2005.07.024
Sadeek, S. A., Mohammed, E. A., Shaban, M., Abou Kana, M. T. H., and Negm, N. A. (2020). "Synthesis, characterization and catalytic performances of activated carbon-doped transition metals during biofuel production from waste cooking oils," *Journal*

of Molecular Liquids 306, article 112749. https://doi.org/10.1016/j.molliq.2020.112749

Samarin, I. A., and Al-Asfour, A. A. (2023). "National human resource development in transitioning societies: The case of Saudi Arabia," *New Horizons in Adult Education and Human Resource Development* 35(1), 20-31. https://doi.org/10.1177/19394225231171157

Sarti, O., El Mansouri, F., Yahia, E. H., Otal, E., Morillo, J., and Saidi, M. (2023). "Efficient removal of tannic acid from olive mill wastewater using carbon steel slag," *C* 9(1), article 32. https://doi.org/10.3390/c9010032

SERA. (2025). "Saudi Electricity Regulatory Authority," Electricity Tariff, https://www.sera.gov.sa/en/systems-and-regulations/electric-tariff.

Tundis, R., Conidi, C., Loizzo, M. R., Sicari, V., Romeo, R., and Cassano, A. (2021). "Concentration of bioactive phenolic compounds in olive mill wastewater by direct contact membrane distillation," *Molecules* 26(6), article 1808. https://doi.org/10.3390/molecules26061808

Wright, M. M., Daugaard, D. E., Satrio, J. A., and Brown, R. C. (2010). "Techno-economic analysis of biomass fast pyrolysis to transportation fuels," *Fuel* 89, S2-S10. https://doi.org/10.1016/j.fuel.2010.07.029

Yahya, M. A., Al-Qodah, Z., and Ngah, C. W. Z. (2015). "Agricultural bio-waste materials as potential sustainable precursors used for activated carbon production: A review," *Renewable and Sustainable Energy Reviews* 46, 218-235. https://doi.org/10.1016/j.rser.2015.02.051

Article submitted: December 31, 2025; Peer review completed: February 21, 2026; Revised version received: March 23, 2026; Accepted: April 4, 2026; Published: April 21, 2026.
DOI: 10.15376/biores.21.2.4977-5009